15 May 2024 21:20:42

RESEARCH ARTICLE | MAY 15 2024

Millimeter-wave and high-resolution infrared spectroscopy of the low-lying vibrational states of pyridazine isotopologues [REE]

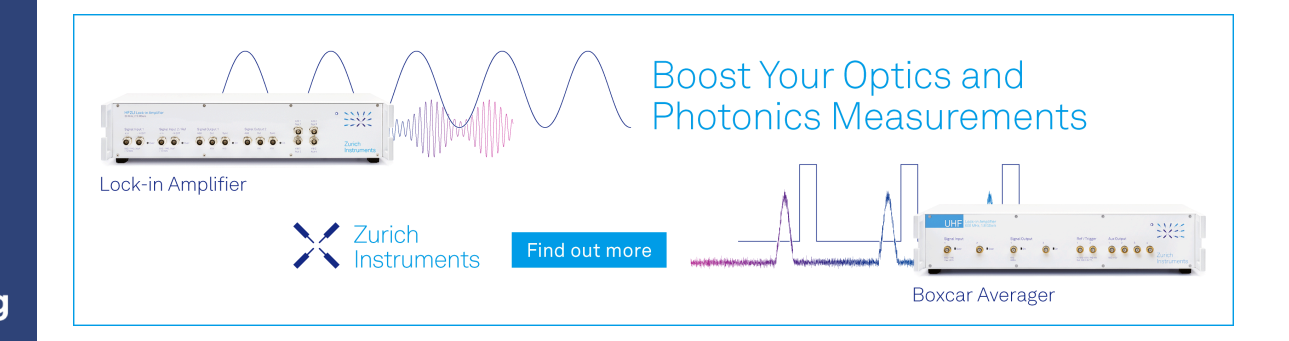
Brian J. Esselman ⁽¹⁾; Maria A. Zdanovskaia ⁽¹⁾; Brent K. Amberger; Joshua D. Shutter ⁽¹⁾; Andrew N. Owen ⁽¹⁾; Brant E. Billinghurst ⁽¹⁾; Jianbao Zhao ⁽¹⁾; Zbigniew Kisiel ⁽¹⁾; R. Claude Woods ⁽²⁾; Robert J. McMahon ⁽²⁾



J. Chem. Phys. 160, 194301 (2024) https://doi.org/10.1063/5.0205488









Millimeter-wave and high-resolution infrared spectroscopy of the low-lying vibrational states of pyridazine isotopologues

Cite as: J. Chem. Phys. 160, 194301 (2024); doi: 10.1063/5.0205488 Submitted: 26 February 2024 • Accepted: 18 April 2024 •







Published Online: 15 May 2024

Brian J. Esselman, D. Maria A. Zdanovskaia, D. Brent K. Amberger, Joshua D. Shutter, D.

Andrew N. Owen, De Brant E. Billinghurst, Dianbao Zhao, Dianbao Zhao, Dianbao Kisiel, Dianbao R. Claude Woods, Dianbao Zhao, Dia



AFFILIATIONS

- Department of Chemistry, University of Wisconsin–Madison, Madison, Wisconsin 53706, USA
- ²Canadian Light Source. Inc., University of Saskatchewan, Saskatoon, Saskatchewan S7N 2V3, Canada
- Institute of Physics, Polish Academy of Sciences, Al. Lotników 32/46, 02-668 Warszawa, Poland

ABSTRACT

The gas-phase rotational spectrum from 8 to 750 GHz and the high-resolution infrared (IR) spectrum of pyridazine (o-C₄H₄N₂) have been analyzed for the ground and four lowest-energy vibrationally excited states. A combined global fit of the rotational and IR data has been obtained using a sextic, centrifugally distorted-rotor Hamiltonian with Coriolis coupling between appropriate states. Coriolis coupling has been addressed in the two lowest-energy coupled dyads (v_{16} , v_{13} and v_{24} , v_{9}). Utilizing the Coriolis coupling between the vibrational states of each dyad and the analysis of the IR spectrum for v_{16} and v_{9} , we have determined precise band origins for each of these fundamental states: v_{16} (B₁) = 361.213 292 7 (17) cm⁻¹, v_{13} (A₂) = 361.284 082 4 (17) cm⁻¹, v_{24} (B₂) = 618.969 096 (26) cm⁻¹, and v_{9} (A₁) = 664.723 378 4 (27) cm⁻¹. Notably, the energy separation in the v₁₆-v₁₃ Coriolis-coupled dyad is one of the smallest spectroscopically measured energy separations between vibrational states: 2122.222 (72) MHz or 0.070 789 7 (24) cm⁻¹. Despite v_{13} being IR inactive and v_{24} having an impractically low-intensity IR intensity, the band origins of all four vibrational states were measured, showcasing the power of combining the data provided by millimeter-wave and high-resolution IR spectra. Additionally, the spectra of pyridazine- d_x isotopologues generated for a previous semiexperimental equilibrium structure (r_e^{SE}) determination allowed us to analyze the two lowest-energy vibrational states of pyridazine for all nine pyridazine- d_x isotopologues. Coriolis-coupling terms have been measured for analogous vibrational states across seven isotopologues, both enabling their comparison and providing a new benchmark for computational chemistry.

Published under an exclusive license by AIP Publishing. https://doi.org/10.1063/5.0205488

INTRODUCTION

The rotational spectrum of pyridazine (o-C₄H₄N₂, $C_{2\nu}$, Fig. 1), the ortho-dinitrogen analog of benzene, has been studied in four previous studies.¹⁻⁴ It was first investigated by Werner *et al.*¹ in 1967 from 9 to 33 GHz. That study determined the rotational, quartic centrifugal distortion, and nuclear quadrupole coupling constants of the ground vibrational state, as well as the dipole moment $[\mu_a]$ = 4.22 (6) D] via the Stark effect. The microwave spectrum from 9 to 15 GHz was reinvestigated by Lopez et al.2 in 2001, refining

the rotational and nuclear quadrupole spectroscopic constants. We provided the first millimeter-wave spectroscopy of pyridazine from 235 to 360 GHz,³ which was later extended to cover the frequency range from 130 to 375 GHz.4 The current work extends the measured spectral range of the ground vibrational state of pyridazine up to 750 GHz, covering a large portion of the frequency range of available radiotelescopes. Like that for many other heteroaromatic compounds, 5-11 the search for pyridazine in the interstellar medium (ISM) has been unsuccessful.⁶ The detection of any heterocyclic aromatic species or their isomers, anions, cations, or radicals,

^{a)}Authors to whom correspondence should be addressed: rcwoods@wisc.edu and robert.mcmahon@wisc.edu

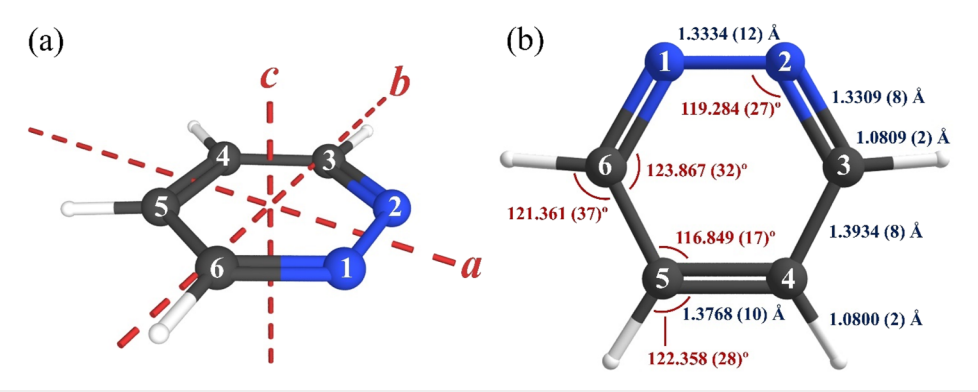


FIG. 1. (a) Pyridazine (o-C₄H₄N₂, C_{2v} , $\mu_{8} = 4.22$ D, 1 $\kappa = 0.824$) with principal axes and atom numbering. (b) Semi-experimental equilibrium structure (r_{e} SE) with 2σ statistical uncertainties.

has the potential to provide substantial insight into the chemistry of the ISM.

A partial substitution structure (r_s) of pyridazine was first determined by Werner et al.1 from four isotopologues, providing the positions of the ring atoms. In the intervening time, substantial improvements have been made in the ability to determine molecular structures. In work pioneered by Boggs and co-workers for the structure of methane in 1978, 12 the differences between the observable rotational constants (B_0) and the equilibrium rotational constants (Be) have been addressed, and the semi-experimental equilibrium structures (r_e^{SE}) for many molecules have been determined. ^{13–16} The first r_e^{SE} structure of pyridazine was reported by Esselman et al.³ using 14 isotopologues. Recently, a new level of agreement has been achieved between experiment and theory for the r_e and r_e SE structures of several molecules, 17-24 including pyridazine. The current best r_e^{SE} structure of pyridazine, using 18 isotopologues measured up to 375 GHz, is reproduced in Fig. 1 with the principal axes indicated. The highly accurate structural parameters are determined with precisions (2 σ) of at least 0.001 Å for bond distances and 0.04 $^{\circ}$ for bond angles. All of the r_e^{SE} structural parameters are in agreement with a high-level theoretical prediction using coupled-cluster calculations, a quintuple-zeta basis set, and additional corrections.

The low-resolution infrared (IR)^{25–29} and Raman spectra² of pyridazine have been studied previously for the normal and several deuterated isotopologues, though the assignments of the vibrational spectra currently in the literature are not consistent for the lowest-energy vibrational states. The rotational spectra of the six lowest-energy fundamental states (<800 cm⁻¹) of the normal isotopologue of pyridazine were previously reported with effective least-squares fits from 235 to 360 GHz.3 The first gas-phase IR and Raman measurements were reported by Ozono et al.,27 who attempted to assign the complete spectrum of pyridazine and pyridazine- d_4 . Pyridazine is a $C_{2\nu}$ molecule with 24 vibrational modes of A₁, A₂, B₁, and B₂ symmetries. The A₂-symmetry modes have an IR intensity of zero, but can be observed in the Raman spectrum. Using Raman spectroscopy, Ozono et al.27 tentatively assigned the two lowest-energy vibrational modes: v₁₃ (A₂, 363 cm⁻¹, liquid) and v_{16} (B₁, 372 cm⁻¹, vapor). The assignment of v_{16} was

supported by the c-type IR spectrum, consistent with a vibration of B₁ symmetry. That work contradicted the previous assignment of v₁₃ to an absorption at 410 cm⁻¹. Ozono et al. also assigned v₉ (A_1) and v_{24} (B_2) to two IR bands at 632 and 663 cm⁻¹, respectively. All four of these IR assignments were later supported by Billes et al.,28 but contradicted by Vázquez et al.,29 who were able to resolve the a-type IR spectral features of v9 in the gas phase and assign it to a mode with A₁ symmetry. With the symmetry inferred from their spectral features, the v_{24} (B₂, 622 cm⁻¹, liquid) and v₉ (A₁, 665 cm⁻¹, vapor) modes were definitively assigned.²⁹ The assignment of these four lowest-energy vibrational modes by Vázquez et al.²⁹ is in reasonable agreement with the CCSD(T)/ccpCVTZ anharmonic frequency calculations for pyridazine provided by Owen et al., which placed the vibrational modes v_{13} (A₂), v_{16} (B_1) , v_{24} (B_2) , and v_9 (A_1) , at 363, 368, 615, and 663 cm⁻¹ respectively. At higher energy, the next three vibrational modes are the two-quanta states associated with v_{13} and v_{16} , which were observed in the spectrum previously,³ but an analysis of these states $(2v_{13}, v_{13})$ + v_{16} , and $2v_{16}$) has not been reported. The vibrational frequencies of these three states are expected to be in the vicinity of v_{15} , from 738 to 747 cm⁻¹, based upon the intensities of their rotational transitions and theoretical estimates.3

Vibrational states v_{12} (A_2) and v_{15} (B_1) are predicted to be very close in energy, but only v_{15} is visible in the IR spectrum. Billes $et\ al.^{28}$ reported an intense c-type IR band centered at 745 cm $^{-1}$, consistent with the B_1 symmetry of v_{15} , which is supported by Vázquez $et\ al.^{29}$ who reported a partially resolved, intense c-type band ranging from 733 to 760 cm $^{-1}$. The frequency of this band is slightly overestimated at 751 cm $^{-1}$ by CCSD(T) calculations. The other vibrational mode, v_{12} , may be the weak Raman-active mode reported by Vázquez $et\ al.^{29}$ at 754 cm $^{-1}$ in the liquid phase. An additional intense c-type IR mode, reported by Billes $et\ al.^{28}$ at 785 cm $^{-1}$, was not observed in any of the other works $^{25-27,29}$ and does not correspond to the computed frequency of any IR-active mode. $^{4,27-29}$ It is likely that this absorption is not from pyridazine, arising from an impurity in the sample or misidentification during data analysis.

While vibrationally excited states v_{13} , v_{16} , v_{24} , v_9 , v_{15} , and v_{12} were previously treated by single-state Hamiltonian models,

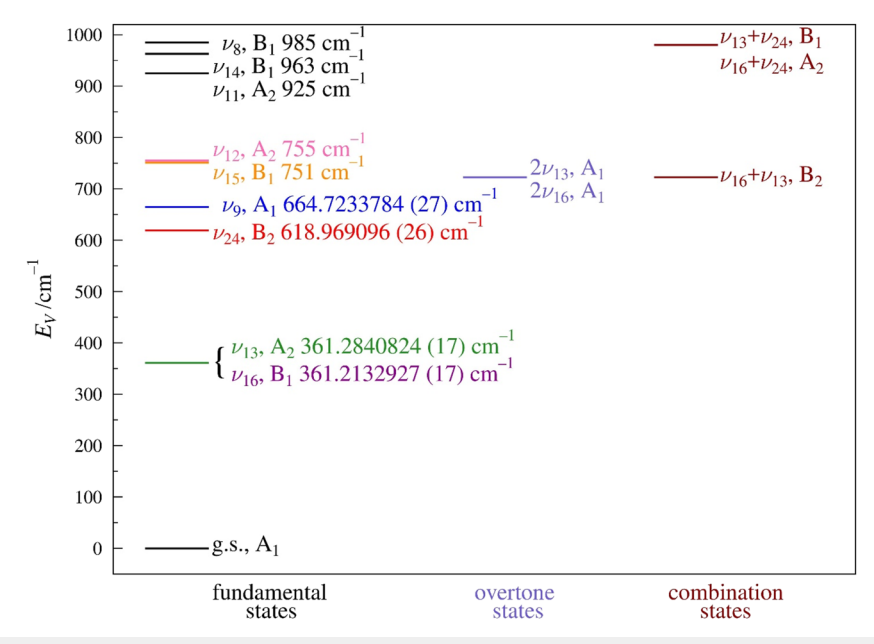


FIG. 2. Vibrational energy levels of pyridazine below 1000 cm⁻¹ using experimental values for ν_{13} , ν_{16} , ν_{24} , and ν_{9} and computed fundamental frequencies [CCSD(T)/cc-pCVTZ] for ν_{15} , ν_{12} , ν_{11} , ν_{14} , and ν_{8} . Combination and overtone state energies are extrapolated from the corresponding experimental fundamental frequencies.

generating effective rotational constants,3 the energy-level diagram (Fig. 2) shows that these states are sufficiently close in energy that complex coupling interactions are expected. Indeed, the previous study noted some clearly perturbed rotational transitions,3 which were excluded from their least-squares fits to obtain rotational and diagonal centrifugal distortion constants that were physically reasonable. Many perturbed transitions may be impacting the spectroscopic constants presented in that work. The current work strives to address the assignment and frequency ambiguities of the previous IR work and to address the Coriolis coupling neglected in the previous rotational spectroscopy work by incorporating high-resolution IR data from the Canadian Light Source (CLS), extending the rotational spectral coverage up to 750 GHz, and utilizing Hamiltonians that include Coriolis coupling. Due to the complex coupling between v_{12} , v_{15} , and the two-quanta vibrational states, an analysis of these states is reserved for future work.

While many works, including every structure determination using rotational spectroscopy, have explored the isotopic dependence of the rotational constants, it has been far less common to explore the impact of isotopic substitution on the vibration–rotation interaction or Coriolis coupling. Several previous works have explored the impact of halogen substitution^{30–36} and deuterium substitution^{37,38} on the vibration–rotation interaction constants, in part due to the ready availability of halogen isotopes at natural abundance or the relative ease of H/D exchange by chemical synthesis. Far fewer studies have looked at the impact of isotopic substitution on the Coriolis coupling between vibrational states.³⁴ The availability of spectra from deuteriated pyridazine samples obtained previously³ provides the opportunity to compare the isotopic dependence on the vibrational energy separations between states, the vibration–rotation

interaction constants, and the Coriolis coupling between analogous states, all of which are provided below.

EXPERIMENTAL METHODS

Rotational spectroscopy

A commercial sample of pyridazine was used without further purification. Using a millimeter-wave spectrometer that has been previously described, 3,24,39 the rotational spectrum of the normal isotopologue of pyridazine was collected from 130 to 230 and from 235 to 360 GHz in a continuous flow at room temperature with a sample pressure of 4 mTorr.³ Additionally, spectral data were obtained with a newly acquired amplification and multiplication chain that extended the frequency range to 750 GHz, with measurements made at a sample pressure of 15 mTorr. The complete spectrum from 130 to 750 GHz was obtained using automated data collection software over approximately two weeks given these experimental parameters: 0.6 MHz/s sweep rate, 10 ms time constant, and 50 kHz AM and 500 kHz FM modulation in a tone-burst design. Additional data in the 8-18 GHz frequency range were collected for the normal isotopologue of pyridazine using a modified waveguide Fouriertransform microwave spectrometer⁴⁰ that was originally constructed in the Kiel laboratory, 41,42 relocated to Warsaw, and subjected to several further modifications. 40,43 The spectra of deuteriated pyridazines used in this work were obtained from 250 to 360 GHz and described in our previous works.^{3,4} A uniform frequency measurement uncertainty of 0.050 MHz was assumed for all measurements from Madison and 0.010 MHz from Warsaw spectrometers.

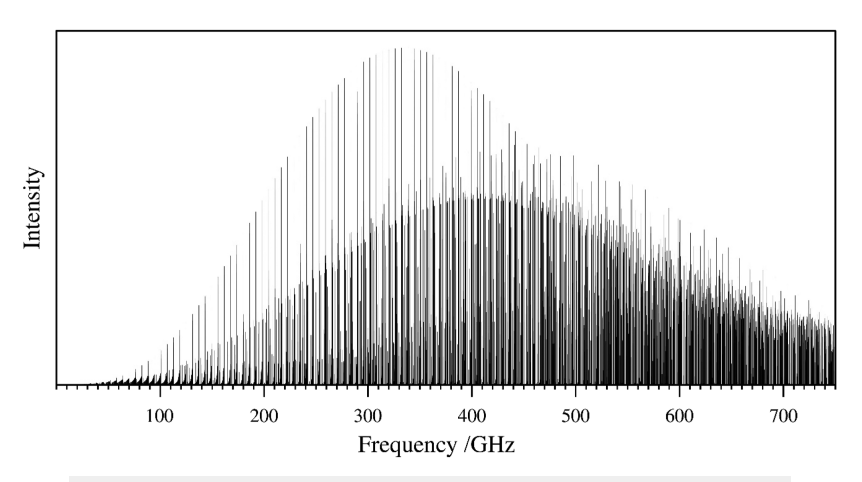


FIG. 3. Predicted rotational spectrum of the ground vibrational state of pyridazine at 292 K.

High-resolution infrared spectroscopy

High-resolution infrared data presented in this work were recorded at the Canadian Light Source (CLS) Synchrotron Far-IR beamline (2020) using a Bruker IFS 125HR spectrometer with synchrotron radiation and a 9.4-m optical path length difference, providing a nominal resolution of 0.000 96 cm⁻¹. The cell is a 2-m, White-type multi-pass cell; the total path length is 72 m. Spectra were collected at room temperature at a series of pressures for the analysis of various vibrational states, which have substantially different infrared intensities. In the range from 400 to 1200 cm⁻¹, spectra were collected at 0.01, 0.045, and 0.071 Torr using a KBr beamsplitter, KBr cell windows, and a Ge:Cu detector housed in a QMC cryogen-free cryostat (cooled by a Cryomech pulsed-tube cooler). The aperture was 1.15 mm and the preamplifier gain of the detector was set to 6×. In the range from 30 to 600 cm⁻¹, spectra were collected at 0.0045 and 0.051 Torr using a 6-micron Mylar beamsplitter, 50-micron polypropylene cell windows, and a superconducting niobium TES bolometer detector. The aperture was 1.5 mm and the preamplifier gain of the detector was set to 6×. A uniform frequency measurement uncertainty of 0.000 18 cm⁻¹ (~6 MHz) was assumed for all infrared measurements.

Spectral analysis

The separate spectral segments were combined into a single broadband spectrum using the Assignment and Analysis of Broadband Spectra (AABS) software. 44,45 Pickett's SPFIT/SPCAT programs 46 were used for least-squares fits and spectral predictions, along with PIFORM, PLANM, and AC programs for analysis. 47,48 In both the vibrational ground and excited states, partially resolved hyperfine splitting was observed. An empirical model was employed to find the hyperfine-removed frequency center. For microwave data, these frequencies were derived by effectively fitting each hyperfine pattern, then calculating the central frequency of those transitions. For millimeter-wave data, the correction was based on the frequencies of the two strongest transitions.

COMPUTATIONAL METHODS

Quantum chemistry computations were carried out using a development version of CFOUR.⁴⁹ Following the optimization of pyridazine using coupled-cluster calculations with single, double, and perturbative triple exictations [CCSD(T)/cc-pCVTZ], harmonic vibrational frequency calculations were carried out for each isotopologue. An anharmonic vibrational frequency calculation was carried out for the normal isotopologue, previously.⁴ All vibrational frequency calculations were performed using second-order vibrational perturbation theory (VPT2), wherein cubic force constants are evaluated by numerical differentiation of analytic first derivatives at displaced points.^{50–52} Computational output files can be found in the supplementary material.

ANALYSIS OF PYRIDAZINE ROTATIONAL SPECTRUM Pyridazine, ground vibrational state

The rotational spectrum of pyridazine from 130 to 750 GHz covers the frequency range of its most intense transitions at ambient conditions. As shown in Fig. 3, the peak intensity for pyridazine transitions occurs around 350 GHz, but the spectral intensity remains strong through 750 GHz. This frequency range allows transitions to be measured for J'' values up to 110 for the ground vibrational state, exceeding the maximum J'' value of the previous work, which only observed transitions up to J'' = 56.³

The rotational spectrum of pyridazine in the observed frequency range is dominated by a-type R-branch transitions, which form typical oblate-top band structures. These bands comprise degenerate $K_a = 0^+$ and 1^- transitions that decrease in J value as they progress away from the bandhead. At moderate K_a , these transitions lose degeneracy, forming doublets of ${}^aR_{0,1}$ transitions. For bands at lower frequency, these transitions progress with decreasing J immediately toward higher frequency, as shown in Fig. 4, but for higher-frequency bands, these transitions progress in the reverse

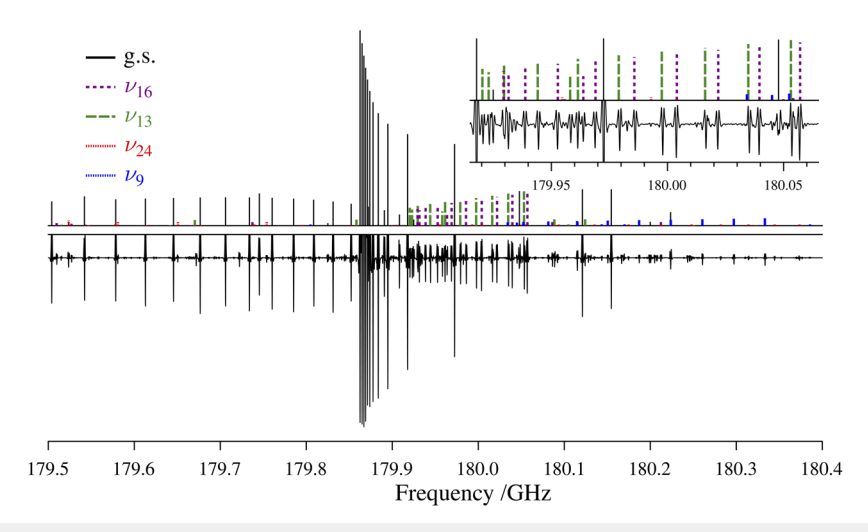


FIG. 4. Experimental rotational spectrum (bottom) of pyridazine from 179.5 to 180.4 GHz and stick spectra (top) from experimental spectroscopic constants with the ground state (black), v_{16} (purple), v_{13} (green), v_{24} (red), and v_{9} (blue). Unlabeled transitions are attributed to higher-energy vibrationally excited states and heavy-atom isotopologues. The inset in the top-right corner shows an expansion of the 179.915–180.065 GHz region for improved visualization of the v_{16} and v_{13} band structures.

direction before turning around and continuing toward higher frequency. Each of the R branches is accompanied by a Q branch where the transitions have $K_{\epsilon}'' = J''$ of the lead R-branch transition.

Over 6200 transitions were assigned, measured, and least-squares fit for the vibrational ground state of pyridazine. Including transitions from previous works, ^{1,3} the dataset consists of R- and Q-branch transitions with J''=0-109 and $K_a{}''=0-67$. The dataset distribution plot is provided in Fig. 5, illustrating this broad spectroscopic coverage. There are a few notable J'' and $K_a{}''$ regions where no or very few transitions are measurable. The diagonal gaps in the R-branch and Q-branch plots are due to gaps in the spectroscopic coverage, while the vertical gaps at low $K_a{}''$ are due to the congestion of many overlapping transitions in the bandhead region.

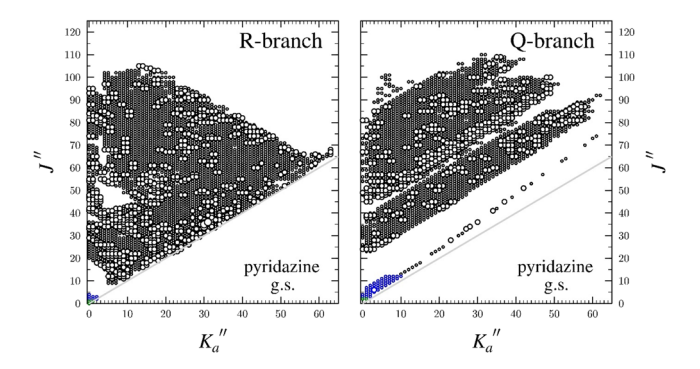


FIG. 5. Data distribution plot for the least-squares fit of spectroscopic data for the vibrational ground state of pyridazine. The size of the outlined circle is proportional to the value of $|(f_{\text{obs.}} - f_{\text{calc.}})/\delta f|$, where δf is the frequency measurement uncertainty, and none of the quotient values are equal to or greater than three. The previously reported transitions appear in blue (Werner *et al.*¹) and green (Lopez *et al.*²).

These gaps are particularly prominent at moderate-to-high ranges of J'', where the bands have multiple turnarounds in their progression. None of these "missing" transitions is due to an untreated coupling with the vibrationally excited states or other systematic errors in the least-squares fit. The transitions are simply unresolvable due to the coincidental overlap of multiple transitions. The transitions included in this work display a partially resolvable hyperfine structure arising from the nuclear quadrupole coupling of each nitrogen atom, as observed previously for low-J transitions in the work of López et al.2 The transitions have been modeled using Aand S-reduced, sextic, distorted-rotor Hamiltonians in the I' and III¹ representations using SPFIT. The spectroscopic constants in the A reduction, I' representation and S-reduction, III' representation (converted from III¹) least-squares fits are provided in Table I, along with their corresponding computed values [CCSD(T)/cc-pCVTZ]. All spectroscopic constants were adequately determined through the sextic level of centrifugal distortion.

Although the III^l representation available in SPFIT is nominally for oblate-top molecules, it was not used here with the A reduction due to its inability to adequately model over 220 correctly assigned R-branch transitions with high K_a and low K_c . These transitions were well-modeled by changing the reduction or representation used for the Hamiltonian, where both least-squares fits had σ_{fit} values of 30 kHz. The breakdown of the A-reduction Hamiltonian is well known for extremely oblate tops, but was not anticipated in this case, where the value of κ for pyridazine is only 0.8235.¹⁹ While the information content in these 220 transitions is likely minor relative to the size of the dataset, rather than exclude them, we have used the established method of changing representation to avoid the breakdown of the A reduction. 53,54 The least-squares fitting output files used, corresponding to Table I, as well as the A reduction, III^l representation, can be found in the supplementary material.

TABLE I. Experimental and computational spectroscopic constants for the ground vibrational state of pyridazine (A- and S-reduced Hamiltonians, I^r and III^r representations, respectively).

	A reduction, I ^r representation			S reduction, III ^r re	presentation
	Experimental	CCSD(T) ^{a,4}		Experimental ^b	CCSD(T) ^{a,4}
A_0 (MHz)	6242.950 982 (24)	6223	A ₀ (MHz)	6242.951 901 (24)	6223
B_0 (MHz)	5961.094 866 (22)	5923	B_0 (MHz)	5961.093 601 (22)	5923
C_0 (MHz)	3048.714 434 (23)	3034	C_0 (MHz)	3048.714 709 (23)	3034
Δ_I (kHz)	0.757 499 0 (55)	0.7378	D_J (kHz)	1.474 509 3 (64)	1.453
Δ_{JK} (kHz)	-0.135 316 (16)	-0.09171	D_{JK} (kHz)	-2.449 537 (12)	-2.413
Δ_K (kHz)	0.829 021 (20)	0.7890	D_K (kHz)	1.100 990 0 (78)	1.083
δ_J (kHz)	0.315 770 5 (23)	0.3075	d_1 (kHz)	-0.0155384(44)	-0.02056
δ_K (kHz)	0.682 753 4 (73)	0.6840	d_2 (kHz)	0.027 199 5 (20)	0.029 38
Φ_{J} (Hz)	0.000 330 07 (58)	0.000 318 4	H_{J} (Hz)	0.000 685 77 (63)	0.000 749 9
Φ_{JK} (Hz)	-0.000 134 1 (33)	-0.0000549	H_{JK} (Hz)	-0.002 690 8 (19)	-0.003081
Φ_{KJ} (Hz)	-0.0012168(78)	-0.001239	H_{KJ} (Hz)	0.003 324 1 (23)	0.003 615
Φ_K (Hz)	0.001 566 2 (62)	0.001470	H_K (Hz)	-0.001 318 8 (11)	-0.001284
ϕ_J (Hz)	0.000 164 95 (28)	0.000 159 2	h_1 (Hz)	-0.00000389(95)	-0.0000080
ϕ_{JK} (Hz)	0.000 267 4 (18)	0.000 295 3	h_2 (Hz)	-0.00004303(65)	-0.0000919
ϕ_K (Hz)	0.001 480 5 (23)	0.0014732	h_3 (Hz)	-0.00002580(16)	-0.0000274
$\Delta_i (u \mathring{A}^2)^{c,d}$	0.036 402 (1)	0.355	$\Delta_i (u \mathring{A}^2)^{c,d}$	0.036381(1)	0.355
κ^{d}	0.823 5	0.812	$\kappa^{\mathbf{d}}$	0.823 5	0.812
$N_{ m lines}^{ m \ e}$	6285		$N_{ m lines}^{ m \ e}$	6285	
$\sigma_{\rm fit}$ (MHz)	0.030		$\sigma_{\rm fit}$ (MHz)	0.030	

^aEvaluated with the cc-pCVTZ basis set.

The spectroscopic constants provided in Table I show the expected agreement between the computed and experimental values for both the A and S reductions. The rotational constants are computed at the CCSD(T)/cc-pCVTZ level to be within 0.3%, 0.6%, and 0.5% of the experimental A_0 , B_0 , and C_0 values, respectively. The computed quartic centrifugal distortion constants are in generally good agreement with the experimental values (within 10%), but in each reduction, one of the computed values (Δ_K and d_1) differs by over 30%. The situation is similar for the sextic centrifugal distortion constants, where most of the constants are in generally good agreement (<10% difference), but in each reduction, one of the constants differs substantially, Φ_{JK} (52%) and h_2 (100%), in the A- and Sreduction fits, respectively. Despite these deviations of the computed values from the experimental ones, the computed spectroscopic constants are adequate for the initial identification of low- K_a transitions in the pyridazine spectrum, even if no previous experimental data were available. The A-reduction constants in the I' representation are used in the analysis of the high-resolution infrared spectrum and the rotational spectra of the vibrationally excited states that follow.

Pyridazine, v_{16} and v_{13}

The two lowest-energy vibrationally excited states of pyridazine $(v_{16}, B_1 \text{ and } v_{13}, A_2)$ form a Coriolis-coupled dyad. Both of these

vibrational states are out-of-plane distortions of the aromatic ring, as depicted previously³ and in Fig. 6. Their transitions are readily visible in Fig. 4, with the closely spaced R-branch transitions in purple and green appearing at a slightly higher frequency than the ground-state transitions, and progressing toward the ground-state R-branch before turning around and progressing to a higher frequency. Initial attempts to adequately model these transitions using

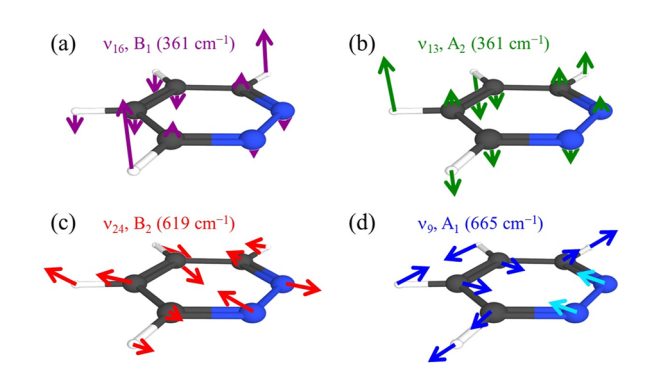


FIG. 6. Vibrational motions of the four lowest-energy vibrationally excited states of pyridazine: (a) ν_{16} , (b) ν_{13} , (c) ν_{24} , and (d) ν_{9} .

^bConverted from III^l in the SPFIT output to III^r.

^cInertial defect, $\Delta_i = I_c - I_a - I_b$.

^dCalculated using PLANM from the B₀ constants.

^eNumber of fitted transition frequencies.

only rotational data in single-state, distorted-rotor models were unsuccessful, though effective rotational constants were provided in the previous work. A two-state, Coriolis-coupled, sextic distorted-rotor Hamiltonian was employed to model the transitions of these two vibrationally excited states, including rotationally resolved infrared transitions of ν_{16} . To incorporate the high-resolution IR data, a global fit was obtained that included the ground vibrational state and the higher-energy Coriolis-coupled dyad of ν_{24} and ν_{9} . The final dataset, which includes over 4500 rotational transitions of ν_{16} and ν_{13} , and over 2600 infrared transitions of ν_{16} , affords a satisfactory least-squares fit with low statistical error ($\sigma_{\rm fit\,ROT}=0.037$ MHz for both ν_{16} and ν_{13} and $\sigma_{\rm fit\,IR}=1.943$ MHz). The spectroscopic constants of ν_{13} and ν_{16} are provided in Table II, alongside constants for the other vibrational states of the global fit.

Due to the incorporation of infrared data and, as a result, the correlation between the ground- and excited-state spectroscopic constants, the ground-state constants presented in Table II are

slightly, but not significantly, different from those presented in Table I. Spectroscopic constants that could not be determined for the vibrationally excited states were held constant at their corresponding values from Table I. The change from ground to v_{16} and v_{13} rotational constants is within 0.1%, and all of the quartic centrifugal distortion constants are within 5% of the corresponding ground-state values. Such small changes suggest that the excited-state constants are physically meaningful and have absorbed minimal perturbation, if any. The sextic centrifugal distortion constants show a larger relative change, as might be expected. All of the sextic values are within 6% of the corresponding ground-state values for v_{16} , with the exception of Φ_{IK} . Φ_{IK} for this state differs from the corresponding ground-state value by ~45%. For v_{13} , three terms differ from their ground-state values by more than 5%: Φ_{JK} (135%), Φ_{KJ} (26%), and ϕ_{JK} (27%). Although these differences stand out from those of the other centrifugal distortion constants, the values of Φ_{KJ} and ϕ_{JK} are likely to be physically meaningful, as they do not correspond to a

TABLE II. Experimental spectroscopic constants for the ground state and vibrationally excited states of pyridazine (A-reduced Hamiltonian, I' representation).

	Ground state ^a	$v_{16} (B_1, 368 \text{ cm}^{-1})^b$	$v_{13} (A_2, 364 \text{ cm}^{-1})^b$	$v_{24} (B_2, 615 \text{ cm}^{-1})^b$	$v_9 (A_1, 664 \text{ cm}^{-1})^b$		
A_{ν} (MHz)	6242.950 961 (29)	6236.126 289 (37)	6240.685 467 (36)	6245.821 84 (16)	6233.595 75 (18)		
B_{ν} (MHz)	5961.094 847 (26)	5961.592 575 (32)	5956.438 468 (31)	5956.682 05 (18)	5963.910 13 (16)		
C_{v} (MHz)	3048.714411 (28)	3052.181778 (24)	3052.128 443 (25)	3047.309 (69)	3046.565 (69)		
Δ_J (kHz)	0.757 495 4 (66)	0.760 176 (11)	0.757 606 1 (98)	0.754 939 (23)	0.762 526 (17)		
Δ_{JK} (kHz)	-0.135312(19)	-0.130743(39)	-0.138 769 (35)	-0.14459(13)	-0.143 86 (15)		
Δ_K (kHz)	0.829 012 (25)	0.813 618 (49)	0.838 494 (51)	0.848 23 (13)	0.807 30 (15)		
δ_J (kHz)	0.3157702 (28)	0.316 499 1 (51)	0.315 187 9 (46)	0.314 767 (16)	0.317 730 (15)		
δ_K (kHz)	0.6827527 (89)	0.682 550 (15)	0.675 079 (15)	0.721 368 (41)	0.635 975 (48)		
Φ_J (Hz)	0.000 329 87 (71)	0.000 327 7 (20)	0.000 323 0 (16)	0.000 351 5 (31)	0.000 256 1 (33)		
Φ_{JK} (Hz)	-0.0001334(40)	-0.000073(11)	-0.000314(10)	$[-0.0001341]^{c}$	$[-0.0001341]^{c}$		
Φ_{KJ} (Hz)	-0.0012179(95)	$-0.001\ 209\ (22)$	-0.000898(23)	-0.004795(44)	0.002 285 (53)		
Φ_K (Hz)	0.001 565 5 (75)	0.001 485 (14)	0.001 492 (16)	0.005 771 (43)	-0.002498(62)		
ϕ_J (Hz)	0.000 164 92 (34)	0.000 162 79 (98)	0.000 162 16 (77)	0.000 175 4 (15)	0.000 127 5 (16)		
ϕ_{JK} (Hz)	0.000 267 5 (22)	0.000 275 0 (49)	0.000 195 3 (51)	$[0.0002674]^{c}$	$[0.0002674]^{c}$		
ϕ_K (Hz)	0.001 480 5 (28)	0.001 549 9 (52)	0.001 417 9 (58)	0.002 217 (13)	0.000 668 (21)		
E (MHz)		10 828 902.088 (51)	0 831 024.310 (51)	8 556 226.68 (78)	19 927 905.550 (82)		
$E (cm^{-1})$		361.213 292 7 (17)	361.284 082 4 (17)	618.969 096 (26)	664.723 378 4 (27)		
G_c (MHz)		1.971 21	(80)	3811 (12)			
F_{ab} (MHz)		-3.667 53	-3.667 53 (12)		2.166 (26)		
$F_{ab}^{\ \ J}$ (MHz)		0.000 01	0.000 016 84 (18)		-0.000 195 8 (28)		
F_{ab}^{K} (MHz)		-0.00000	08 91 (21)	-0.000 191 76 (92)			
$\Delta_i (u \mathring{A}^2)^d$	0.036403(2)	-0.233 428 (2)	-0.244 683 (2)	0.087 2 (38)	0.0719 (38)		
$N_{\rm lines} { m ROT}^{ m e}$	6264	4533	4619	3248	2771		
$N_{\rm lines}$ IR ^e	3603	2646			957		
σ _{fit} ROT (MHz)	0.031	0.037	0.037	0.044	0.047		
σ _{fit} IR (MHz)		1.943			1.985		

^aSpectroscopic constants differ slightly from the single-state constants presented in Table I; see text.

^bFundamental frequencies calculated using CCSD(T)/cc-pCVTZ. Color-coding designates the type of vibrational motion (see Fig. 6) and not the vibrational state label.

^cValue held constant at ground-state value from Table I.

^dInertial defect, $\Delta_i = I_c - I_a - I_b$. Calculated using PLANM from the B_v constants.

^eNumber of fitted transition frequencies

similar behavior in v_{16} . The somewhat large and opposite-direction changes in the Φ_{JK} values more likely indicate some absorption of coupling into these terms. The best means to draw a conclusion as to whether these terms have inappropriately absorbed coupling, however, would be to compare them to computed constants (not readily available by any software). The energy separation determined by the coupling analysis is very small [2122.222 (72) MHz or 0.070 789 7 (24) cm⁻¹] and, importantly, indicates that v_{16} and v_{13} are in the opposite order than that predicted by CCSD(T)/cc-pCVTZ, *i.e.*, v_{16} is actually lower in energy than v_{13} .

The computed changes in the rotational constants $(B_0 - B_\nu)$ for v_{16} and v_{13} at the CCSD(T)/cc-pCVTZ level are in very close agreement with their corresponding experimental values, better than often seen for a Coriolis-coupled dyad of vibrational states (Table III). 55,56 This close agreement provides confidence both that the experimental values are physically meaningful and that the computed geometry and force constants are accurately predicted at the theoretical level. In part, the close agreement of the experimental and computed values is a consequence of the vibrational motions of v_{16} and v_{13} . While the symmetries of these two vibrational states allow c-axis coupling, the out-of-plane motions of v_{13} (A₂) and v_{16} (B_1) for this planar molecule do not result in a typical G_c constant that arises from a corresponding Coriolis (ζ) constant (vide infra). For these fundamental states, the c-axis Coriolis ζ value is equal to zero. This circumstance has been observed for other planar molecules with coupled, out-of-plane modes, e.g., v_{14} (B₂) and $v_{11}(A_1)$ of furan.^{57,58} The *c*-axis Coriolis constant used in the two previous works on furan, F_{ab} (labeled G_c and C_{corr} in those works, respectively), was able to adequately model the interaction between these analogous vibrationally excited states when combined with their centrifugal distortion terms. 57,58 While a G_c value was used for pyridazine, it is relatively small and results from higher-order contributions to the Coriolis-coupling coefficient than accounted for in the ζ constant. Given the small value of the G_c constant, it is not surprising that the experimental and computed $B_0 - B_v$ constants appear to be unperturbed and are largely free of the effects of unaddressed Coriolis coupling. This analysis is supported by the close agreement between the experimental vibration–rotation interaction constants from the previous work, where noticeably perturbed transitions were excluded to obtain effective least-squares fits, and those from this work, where the Coriolis coupling was explicitly treated.

The very small energy difference between v_{13} and v_{16} , only 0.070 789 7 (24) cm⁻¹, makes it *a priori* very likely that the energy levels of these states will mix and prevent these states from being reasonably treated with a single-state Hamiltonian. This energy gap can be determined only from the rotational data, since v_{13} has no infrared intensity. Neither band origin, however, is determinable without the observation of rotationally resolved infrared transitions of v_{16} , since neither state is coupled to the ground state. The final fit included a few transitions associated with small resonances and many transitions impacted by the Coriolis coupling, but the high-quality determination of the energy gap and spectroscopic constants for these states can be attributed to the inclusion of nearly 150 nominal interstate transitions. These transitions occur

TABLE III. Vibration-rotation interaction and Coriolis-coupling constants of pyridazine dyads.^a

	Experimental (this work)	CCSD(T) ^{b,4}	obscalc.	Experimental (previous work) ³
A_0 – A_{16} (MHz)	6.824 672 (47)	6.93	-0.10	6.823 0 (69)
$B_0 - B_{16} \text{ (MHz)}$	-0.497728(41)	-0.52	0.02	-0.4946(63)
C_0 – C_{16} (MHz)	-3.467 367 (37)	-3.40	-0.07	-3.466 28 (31)
$A_0 - A_{13} \text{ (MHz)}$	2.265 494 (46)	2.26	0.01	2.0845 (90)
$B_0 - B_{13} \text{ (MHz)}$	4.656 379 (40)	4.58	0.08	4.822 1 (80)
C_0 – C_{13} (MHz)	-3.414 032 (38)	-3.40	-0.02	-3.415 19 (33)
$A_0 - A_{24} \text{ (MHz)}$	-2.870 88 (18)	-3.15	0.28	-2.877 90 (64)
$B_0 - B_{24} \text{ (MHz)}$	4.412 80 (20)	4.18	0.23	4.420 37 (57)
C_0 – C_{24} (MHz)	1.405 (69)	11.09	-9.69	11.993 62 (28)
A_0 – A_9 (MHz)	9.355 21 (18)	10.04	-0.689	9.344 97 (30)
B_0 – B_9 (MHz)	-2.815 28 (16)	-3.05	0.23	-2.80707(30)
C_0 – C_9 (MHz)	2.149 (69)	-7.59	9.73	-8.4384 (22)
$\frac{(A_0-A_{24})+(A_0-A_9)}{2}$ (MHz)	3.242 17 (24)	3.45	-0.20	3.233 53 (71)
$\frac{(B_0-B_{24})+(B_0-B_9)}{2}$ (MHz)	0.79876 (24)	0.57	0.23	0.806 65 (65)
$\frac{(C_0 - C_{24}) + (C_0 - C_9)}{2}$ (MHz)	1.78 (10)	1.75	0.02	1.777 6 (22)
$ \zeta_{24,9}^c $	-0.632 2 (39)	-0.620	-0.01	

^aColor-coding designates the type of vibrational motion (see Fig. 6) and not the vibrational state label.

^bEvaluated with the cc-pCVTZ basis set.

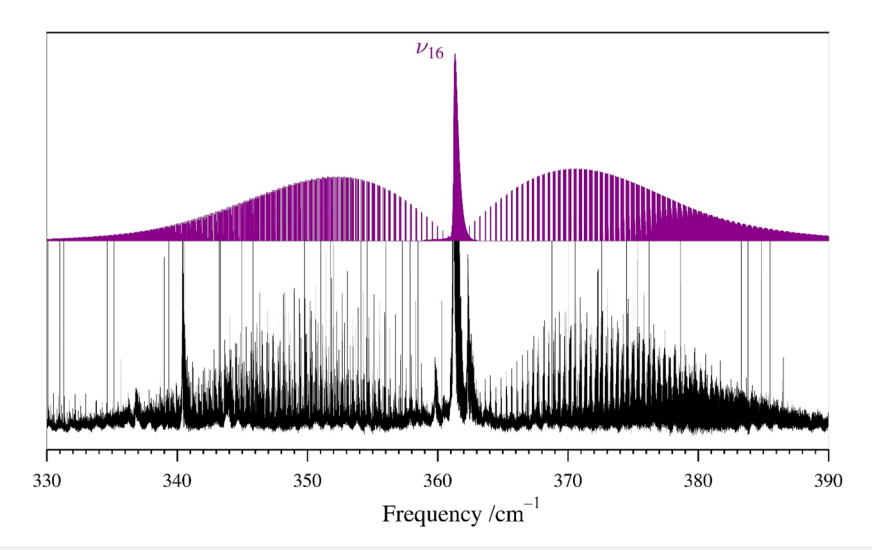


FIG. 7. Predicted stick spectrum of v₁₆ (purple, top) and the experimental high-resolution infrared spectrum (bottom) of pyridazine from 330 to 390 cm⁻¹.

between highly mixed rotational energy levels and allow for normally forbidden transitions with simultaneous change of rotational and vibrational quantum number to occur. The Coriolis coupling between ν_{16} and ν_{13} and the high-resolution infrared analysis of ν_{16} allow the energy of ν_{13} to be accurately and precisely determined [361.284 082 4 (17) cm⁻¹] despite the fact that ν_{13} is not directly observed in the infrared or Raman spectra. Our analysis confirms the assignment of ν_{13} (A₂, 363 cm⁻¹, liquid) by Ozono *et al.*²⁷ and not the value at 410 cm⁻¹.²⁶ The gas-phase band origins of ν_{16} reported by Ozono *et al.* and Billes *et al.*²⁸ (372 and 369 cm⁻¹, respectively)

are in poorer agreement with the value determined in this work [361.213 292 7 (17) cm $^{-1}$]. The origin of this disagreement is not clear, though the disagreement may be due to the observed slope of the baseline at the edge of the instrumental frequency range of the previous work. 27 As shown in Fig. 7, the band origin for ν_{16} is unambiguously at 361 cm $^{-1}$.

An example of the small resonances and their accompanying coupling-allowed, nominal interstate transitions is provided in Fig. 8. The energy levels $35_{27,9}$ for ν_{16} and $35_{26,9}$ for ν_{13} are separated by only 298 MHz, which results in intense state mixing and allows

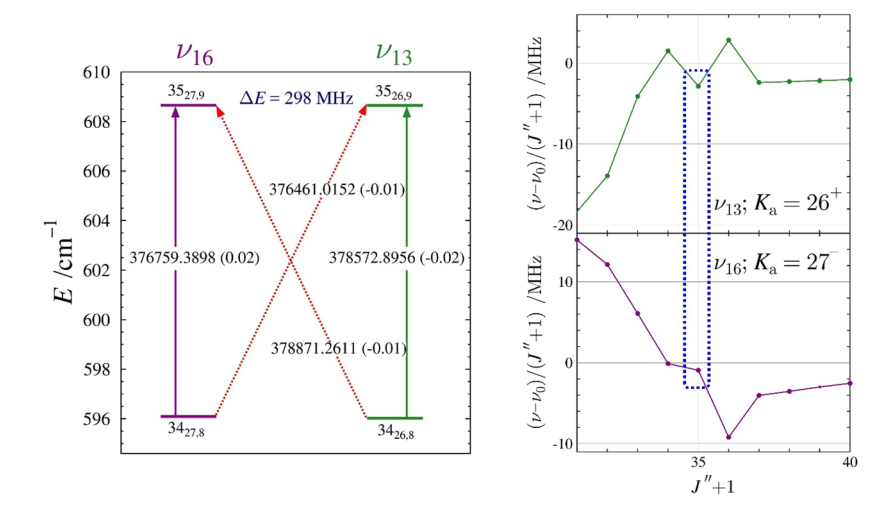


FIG. 8. Energy diagram (left) depicting a representative matched pair of nominal interstate transitions between the v_{16} (purple) and v_{13} (green) vibrationally excited states of pyridazine. Standard ${}^aR_{0,1}$ transitions within vibrational states are denoted by vertical arrows. The diagonal, dashed arrows indicate nominal interstate transitions that are formally forbidden, but allowed as a result of rotational energy-level mixing. The values printed on each of the arrows are the corresponding transition frequency (in MHz) with the corresponding *obs.-calc*. value in parentheses. The marked energy separation is between the two strongly interacting rotational energy levels. Resonance plots (right) of the K_a series of v_{16} and v_{13} show the corresponding resonant intrastate transitions.

the observed interstate transitions between v_{16} and v_{13} . This same state mixing also causes a perturbation in the observed frequency of the corresponding in-state ^aR_{0.1} transitions by about 100 MHz. All four of these transitions have obs.-calc. values of less than 25 kHz, which is less than half of the assumed experimental measurement uncertainty of 50 kHz. Additionally, the averages of the experimental frequencies of the intrastate transitions and the interstate transitions differ by less than 5 kHz, which is probably fortuitously small. Nevertheless, this close agreement provides high confidence that these transitions are correctly assigned and measured. These checks can be quite important for species that have moderate state mixing, as the nominal interstate transition intensities may be quite small. Alternately, for species with intense state mixing, the intensities of the intrastate transitions may be quite small due to intensity borrowing by the interstate transitions. The latter is the case for v_{16} and v_{13} , where the intensity borrowing is sufficient that a large number of nominal interstate transitions were able to be measured, assigned, and included in the least-squares fit. In a fashion not typical of Coriolis-coupled dyads, we were able to identify an entire series of interstate transitions via Loomis-Wood plots, as shown in Fig. 9. As mentioned, the combined effect of having many resonant and nominal interstate transitions is that the energy difference between v₁₆ and v₁₃ is very precisely and accurately known. Combined with the rotationally resolved infrared transitions for v_{16} , the band origins for both vibrationally excited states are extremely well determined.

Pyridazine, v_{24} and v_9

The next-lowest energy vibrationally excited states after ν_{16} and ν_{13} are ν_{24} (B₂) and ν_{9} (A₁), respectively, and these, too, comprise a Coriolis-coupled dyad. As depicted in Fig. 6, the ν_{24} and ν_{9} vibrations involve in-plane distortions of the pyridazine ring. The ν_{24} / ν_{9} dyad is included in a global least-squares fit that also includes the ground state, ν_{16} , ν_{13} , and incorporates both millimeter-wave

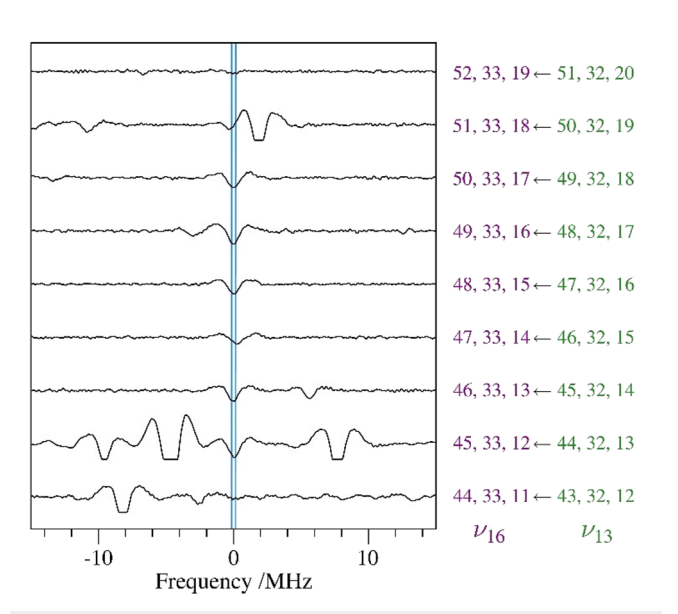


FIG. 9. Loomis–Wood plot of a *b*-type series ($K_a^{\prime\prime}=32$) of nominal interstate transitions between ν_{13} and ν_{16} of pyridazine.

and infrared data (Table II). The transition intensities of v_{24} and v_9 are so much smaller than the lower-energy v_{16} - v_{13} dyad that the former is barely discernible in Fig. 4, but is nonetheless sufficiently intense for the coupling analysis. Transitions of v_{24} and v_9 were also readily seen in the centimeter-wave spectra (Warsaw), providing access to a different range of quantum numbers than at millimeter and submillimeter-wave frequencies (Madison). As shown in Fig. 10, v_9 displays the typical a-type band structure in the infrared range, consistent with a mode of A_1 symmetry. While v_{24} is a nominally infrared active mode with B_2 symmetry, its intensity is too low for transitions to be measured or assigned. Some of our data have a

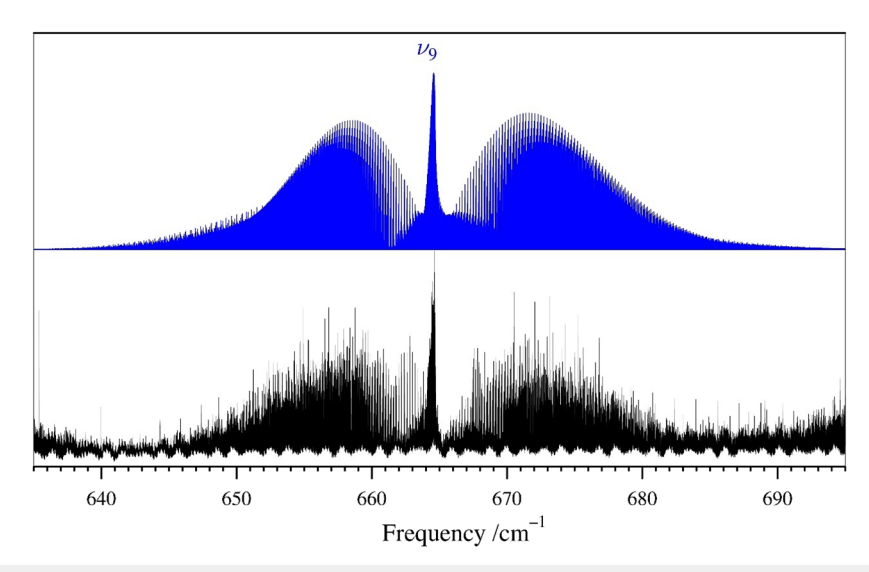


FIG. 10. Predicted stick spectrum of v₉ (blue, top) and the experimental high-resolution infrared spectrum (bottom) of pyridazine from 635 to 695 cm⁻¹.

non-pyridazine impurity in the vicinity of ν_{24} , potentially obscuring its transitions. It is possible that a future intentional search for this weak fundamental could be successful.

In contrast to v_{16} and v_{13} , which are very close in energy, v_{24} and v_9 are separated by a much larger energy difference, 45.754 282 (26) cm⁻¹. The Coriolis-coupling interaction between these two vibrationally excited states becomes apparent in the frequencies of the ^aR_{0.1} transitions in the extended millimeter-wave frequency range incorporated in this work, despite the larger energy separation. As a result, a two-state, sextic centrifugally distorted Hamiltonian model was applied to these vibrationally excited states. The smaller number of measured transitions for these higherenergy states prevented the determination of Φ_{IK} and ϕ_{IK} in the least-squares fitting (Table II). The quartic centrifugal distortion constants are similar to those of the ground state, with the largest deviations being less than 7%. These changes are of the expected magnitude for even a single-state fit of an uncoupled vibrationally excited state, indicating that the quartic centrifugal distortion constant values are likely well determined and physically meaningful. A few of the sextic centrifugal distortion constants, however, change dramatically relative to the ground state, particularly Φ_{KI} and Φ_{K} for both states. These constants (Table II) should be viewed as highly effective and likely not physically meaningful, especially due to the fact that the observed changes from the ground-state values are similarly large (over 250%) and in opposite directions for the two states—a hallmark of coupling absorbed into spectroscopic terms. Due to the change in representation and reduction between the previous work and this one, the comparison of the determined spectroscopic constants is not straightforward beyond the rotational constants. The rotational constants (Table III) are in reasonable agreement with those determined previously from an effective fit and those determined in this work from a two-state, Corioliscoupled Hamiltonian, with the exception of C_{24} and C_9 . While the small changes in A_{ν} and B_{ν} may be largely attributable to the change in reduction and representation of the two least-squares fits, the changes in C_{ν} are far too large. These differences are due to the nature of the Hamiltonian model used in each least-squares fit. Both the computed and previous experimental C_0 – C_ν values are perturbed by the untreated Coriolis coupling inherent in those values, resulting in good agreement between these values. The C_0 – C_ν values from this work are largely free of the impact of Coriolis coupling and are much closer together than the perturbed values from the previous fit. There is a strong correlation between $G_{24,9}^c$ and the C_{ν} values, which complicates this analysis. The computed $|\zeta_{24,9}^c|$ value of -0.620is in very good agreement with the experimentally determined value of -0.6322 (39), validating the computed value and providing a strong indicator that the experimentally determined value is physically meaningful. The averaged vibration-rotation interaction values are in excellent agreement (within 30 kHz), indicating the quality of the computational estimates of this average and the ability of the Hamiltonian model to treat the transitions included in the dataset.

While the coupling between v_{24} and v_9 complicates the analysis and least-squares fitting of their transitions, it does allow the band origin of v_{24} to be determined, despite the very low infrared intensity of this fundamental state. The nearly 960 rotationally resolved transitions of the v_9 band provide an excellent determination of its band origin at $664.723\,378\,4\,(27)\,\mathrm{cm}^{-1}$, which through Coriolis coupling places the v_{24} band origin at $618.969\,096\,(26)\,\mathrm{cm}^{-1}$. We

were unable to assign rotationally resolved infrared transitions for v_{24} . The infrared frequency of v_9 is in good agreement with the previously reported gas-phase values of 663 cm⁻¹ from Ozono *et al.*²⁷ or 665 cm⁻¹ from Vázquez *et al.*²⁹ but disagrees somewhat with the more recent report of 673 cm⁻¹ from Billes *et al.*²⁸ Given the strong intensity of this vibration in the gas phase, it is not surprising that the previous low-resolution gas phase measurements were able to determine the vibrational frequency within 1 or 2 cm⁻¹. The vibrational frequency of v_{24} was previously reported at 622 and 632 cm⁻¹ (Ozono *et al.*,²⁷ crystal Raman and infrared spectroscopy, respectively), 622 cm⁻¹ (Billes *et al.*,²⁸ vapor), and 622 cm⁻¹ (Vázquez *et al.*,²⁹ vapor-phase), with the latter two values agreeing reasonably well with the more precise measurements made in this work.

The Coriolis coupling that is responsible for the accurate and precise energy determination of v_{24} creates many c-type resonances between v_9 and v_{24} , as shown in Fig. 11. These resonances are quite small across the frequency range of this work, with the transitions shown in Fig. 11 displaced by less than 1 MHz. The displacement of these transitions grows in intensity as J'' increases (Fig. 12), but it never achieves the intense perturbation of transitions observed in many other Coriolis-coupled dyads. ^{55,56,59-66} The largest displacement of a resonant transition included in the dataset is only ~240 MHz from its predicted location without accounting for perturbation. The small displacements initially made it challenging for SPFIT to determine the Coriolis-coupling coefficients in the least-squares fitting. The values of $G_{24,9}^c$ and E_{24} were manually adjusted

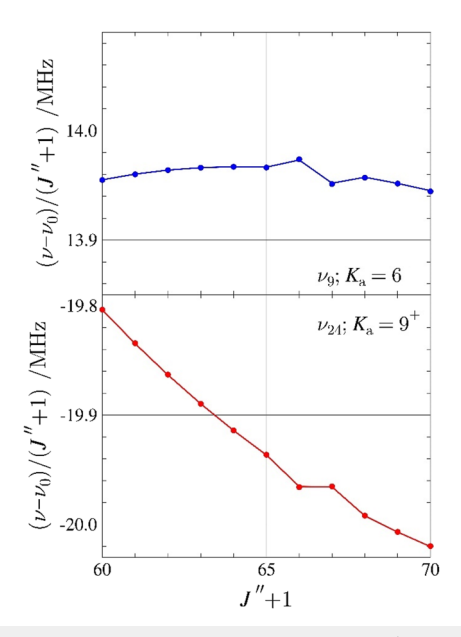


FIG. 11. Resonance plots for pyridazine showing the $K_a=9^+$ series for ν_{24} and the $K_a=6^-$ series for ν_9 . These two resonances conform to the $\Delta K_a=3$ selection rule for c-type resonances. The plotted values are frequency differences between excited-state transitions and their ground-state counterparts $(\nu-\nu_0)$, scaled by (J''+1) in order to make the plots more horizontal. Measured transitions are represented by circles: ν_{24} (red) and ν_9 (blue). No transitions have obs.-calc. values exceeding 150 kHz or three times the nominal experimental measurement uncertainty. Predictions from the final least-squares fit are represented by solid, colored lines

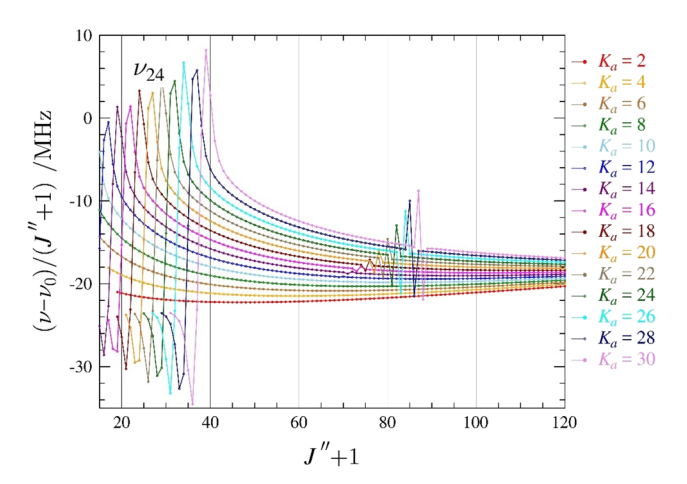


FIG. 12. Superimposed resonance plots of v_{24} for ${}^aR_{0,1}$ even- K_a^+ series from 2 to 30 for pyridazine. Measured transitions are omitted for clarity, but they are indistinguishable from the plotted values on this scale. The plotted values are frequency differences between excited-state transitions and their ground-state counterparts $(v-v_0)$, scaled by (J''+1).

until the fit reasonably modeled the mildly displaced transitions. As additional perturbed transitions were added to the dataset, the four coupling parameters and the energy of v_{24} were allowed to vary in the least-squares fitting. Not surprisingly, the small displacement of the resonant transitions coincides with very little intensity borrowing from those intrastate transitions into the nominal interstate transitions. For this dyad, no nominal interstate transitions were observed. As a result of the small displacements of the resonant transitions and the lack of interstate transitions, the value of $G_{24.9}^c$ [3811 (12) MHz] is determined with only a modest level of precision. Nevertheless, the computed $|\zeta_{24,9}^c|$ value and that determined from the experimental $G_{24,9}^c$ value are in good agreement, differing by 0.01 (less than 2%), indicating that the accuracy of this parameter is as good as normally expected. Note that even though both of the dyads studied here involve *c*-axis Coriolis coupling interactions, $|\zeta_{24,9}^c|$ is expected to be non-zero because v_{24} and v_9 are both in-plane motions, whereas $|\zeta_{16,13}^c|$ must be zero, as both of those vibrations are out-of-plane motions.

Spectral analysis of pyridazine- d_x fundamental states

The aforementioned availability of experimental spectral data for the deuteriated isotopologues of pyridazine and the preceding analysis of v_{13} and v_{16} for the normal isotopologue provide a unique opportunity. With the exception of very small molecules or halogenated compounds, the isotopic differences in the vibrational excited states of compounds are difficult to explore by rotational spectroscopy due to the low natural isotopic abundances. The deuterium-enriched pyridazines present in three different samples of varying composition recorded previously allow the lowest-energy vibrationally excited states (v_{13} and v_{16} for the $C_{2\nu}$ species or v_{24} and v_{23} for the C_s species) to be easily observed at ambient conditions. The coupling observed for these vibrational states in the normal isotopologue changes in several important ways by isotopic substitution. For some isotopologues, the symmetry changes

from $C_{2\nu}$ to C_s , changing the symmetries of the vibrational modes and the allowed coupling interactions without substantially changing the actual vibrational motions. The orientation of the principal axes may change upon isotopic substitution, causing changes in the magnitude of the a-axis and b-axis dipole moment components. For example, the normal isotopologue has only an a-axis dipole moment, while [3,4,5,6-2H]-pyridazine has only a b-axis dipole moment, resulting in only b-type transitions. Additionally, the H/D substitution differentially impacts the vibrational energies of each mode. Given the near degeneracy of v_{16} and v_{13} in the normal isotopologue, it is the specific isotopic substitution pattern that determines which vibrational motion will be lower in energy. These energy changes have a substantial impact on the magnitudes of the observed Coriolis interactions between the lowest-energy fundamental states. Figure 13 shows the evolution of the vibrational modes of pyridazine below 800 cm⁻¹ from the all-protio to the all-deuterio isotopologue. The experimental fundamental energies are used for the experimentally observed states of pyridazine (v_{13} , v_{16} , v_{24} , and v_9), while the vibrational energies for all other vibrational states are their harmonic values computed at the CCSD(T)/cc-pCVTZ level. For the $C_{2\nu}$ isotopologues, the symmetries of v_{13} and v_{16} (A₂ and B₁, respectively) are sufficient to differentiate the atomic motions of the vibrational modes. As mentioned previously, both of these vibrations are out-of-plane ring deformations. When these same molecular motions occur for the C_s isotopologues, the A" symmetries do not distinguish the molecular motions. The Cartesian coordinates of the normal coordinates of each vibrational mode were used to identify analogous vibrational motions across isotopologues, regardless of the idiosyncrasies of their state labels. In Fig. 13 and throughout the article, the same color is used to label the analogous vibrational modes.

The Coriolis coupling observed for v_{13} and v_{16} in the normal isotopologue is evident between the analogous fundamental states (v_{24} and v_{23} or v_{13} and v_{16} for C_s and $C_{2\nu}$ isotopologues, respectively) for six of the nine possible deuteriated pyridazines in the observed frequency range. The three isotopologues ([3,4-2H]-, [3,6-2H]-, and [3,4,6-2H]-pyridazine) for which the lowest-energy fundamental states do not display clear evidence of Coriolis coupling (curvature of series, intensity borrowing, resonant transitions, or nominal interstate transitions) all have predicted energy separations of greater than 24 cm⁻¹. For all of the other deuteriated species (both C_s and $C_{2\nu}$), noticeable perturbations of transitions due to Coriolis coupling are evident in their spectra between 250 and 360 GHz. Due to the combined limitations of relatively low numbers of available transitions and expected complex coupling interactions for the next lowest-energy fundamental states for the pyridazines- d_x (corresponding to v_9 and v_{24} in the normal isotopologue), an analysis of these vibrationally excited states was not undertaken.

For both $[3-^2H]$ - and $[4-^2H]$ -pyridazine, v_{24} and v_{23} present large resonances in their lowest- K_a series in the observed spectral range, in contrast to the analogous vibrational modes of the normal isotopologue. These resonances arise due to the vibrational energy spacing of these modes, as well as their Coriolis-coupling coefficient values. The assignment, measurement, and initial least-squares fitting of the low- K_a R-branch series for these fundamental states was relatively straightforward using the rotational constants of their parent isotopologue and their CCSD(T)-predicted vibration-rotation interaction constants. Due to the limited

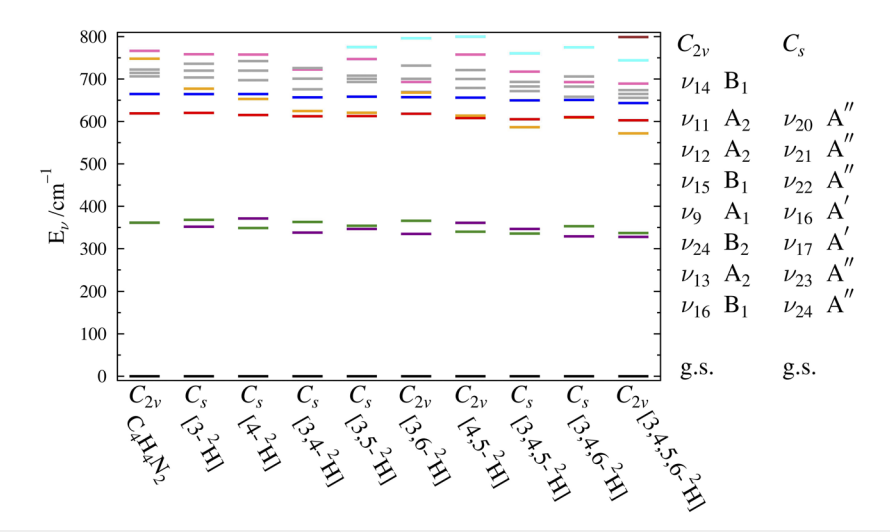


FIG. 13. Vibrational energy levels of pyridazine below 800 cm⁻¹ and the corresponding modes of the deuteriated isotopologues. Fundamental energies for the normal isotopologue are those determined in this work (experimental for v_{13} , v_{16} , v_{24} , and v_{9} ; computed for v_{15} and v_{12}). On this scale, the energies of v_{13} and v_{16} of the normal isotopologue are indistinguishable. All other vibrational energies are harmonic frequencies [CCSD(T)/cc-pCVTZ]. Two-quanta states are depicted in gray. Color-coding designates the type of vibrational motion (see Fig. 6) and not the vibrational state label. The vibrational state labels of v_{16} and v_{13} apply only for the case of $C_{2\nu}$ isotopologues of pyridazine. Vibrational state labels change as a function of isotopic substitution for reasons of both symmetry and isotopic perturbation of vibrational modes.

spectral coverage (250-360 GHz) for these isotopologues, which greatly reduced the K_a series available compared to the normal isotopologue, the initial least-squares fitting of transitions at or near the resonances in the lowest- K_a series was challenging. Without the large undulations of the K_a series observable across many Jquanta that typically provide initial constraints on the energy difference and coupling constants, the fitting of these dyads required manual adjustments of the energy difference and F_{ab} to allow confident assignment of transitions associated with the resonances. With preliminary modeling of the resonances in this manner, the leastsquares fitting of the datasets for each isotopologue was relatively straightforward and resulted in the spectroscopic constants presented in Table IV. Least-squares fitting files, summaries of the spectroscopic constants determined for each isotopologue in its ground and two vibrationally excited states, and dataset distribution plots are provided in the supplementary material.

Despite an excellent model for reproducing the measured transition frequencies for v_{24} and v_{23} of $[3^{-2}H]$ - and $[4^{-2}H]$ -pyridazine, the measurement of transitions is complicated by the spectral density of the available datasets. These spectra were convenient for obtaining spectroscopic constants for all of the pyridazine- d_x isotopologues from only three syntheses and broadband data collections. That convenience for structure elucidation, however, necessitates that there are several abundant isotopologues in each spectrum, resulting in many overlapping transitions from the various isotopologues and vibrationally excited states of multiple pyridazine- d_x isotopologues present. Additionally, the slower, base-catalyzed H/D exchange at the 3-position of pyridazine produced a low concentration of $[3^{-2}H]$ -pyridazine in all samples. This resulted in a dataset about four times smaller than for $[4^{-2}H]$ -pyridazine. Despite these limitations, the least-squares fit of the available datasets for both

isotopologues provides precise and accurate measurements of the energy separation between the fundamental states ($\Delta E_{23,24}$), showing that the isotopic substitution greatly increased the energy difference between the vibrational modes [19.736276 (40) cm⁻¹ and 19.912 797 4 (37) cm⁻¹ for [3-²H]- and [4-²H]-pyridazine, respectively] relative to that of the normal isotopologue. Due to the limited dataset and frequency range, the A_{ν} and B_{ν} values of v_{24} and v_{23} for [3-2H]-pyridazine are highly correlated, as is evident from their lessprecise determination. Efforts to reduce the correlations between spectroscopic constants by either removing them or holding them at their predicted values while still adequately fitting the wellassigned transitions were unsuccessful in those fits with such correlations. Therefore, the most reliable values determined for [3-2H] -pyridazine are likely to be the energy gap and coupling parameters, due to the inclusion of the resonant and nominal interstate transitions in these datasets.

The experimental and computed vibration–rotation interaction constants are displayed in Table V for all nine deuteriopyridazines. The change in the rotational constants for the two lowest-energy fundamental states is well predicted for each isotopologue at the CCSD(T)/cc-pCVTZ level. Typically, the averages of the vibration-rotation interaction constants for coupled states display much better agreement between experimental and computed values than the individual interaction constants. In this case, the agreement between experimental and computed values for the individual interaction constants is also quite good - comparable to the agreement between experimental and computed values for the averaged constants (Table V). For all of the $C_{2\nu}$ isotopologues, this agreement is likely due to the absence of a large G_c term in the Coriolis interaction (as with ν_{13} and ν_{16} of the normal isotopologue) and the treatment of the coupling with F_{ab} . The largest relative errors in the predicted

TABLE IV. Experimental spectroscopic constants for vibrationally excited states v_{24} and v_{23} of [3-2H]- and [4-2H]-pyridazine (A-reduced Hamiltonian, If representation).

	[3- ² H]-pyridazine		[4- ² H]-p	H]-pyridazine		
	$v_{24} (A'', 352 cm^{-1})^{c}$	$v_{23} (A'', 368 cm^{-1})^{c}$	$v_{24} (A'', 349 cm^{-1})^{c}$	$v_{23} (A'', 371 cm^{-1})^{\circ}$		
A_{ν} (MHz)	5960.698 (52)	5959.091 (48)	6188.610 53 (14)	6185.376 70 (18)		
B_{ν} (MHz)	5822.918 (50)	5825.102 (46)	5594.105 14 (10)	5598.934 98 (13)		
C_{ν} (MHz)	2949.883 04 (37)	2949.919 03 (37)	2942.735 148 (63)	2942.867 378 (65)		
Δ_I (kHz)	0.679 27 (11)	0.680 17 (11)	0.668 327 (48)	0.671 979 (59)		
Δ_{IK} (kHz)	[-0.173]	[-0.173]	-0.224 14 (16)	-0.236 09 (19)		
Δ_K (kHz)	0.8821 (18)	0.8840 (18)	1.026 75 (12)	1.030 03 (14)		
δ_I (kHz)	[0.281]	[0.281]	0.275 941 (23)	0.277 649 (29)		
δ_K (kHz)	[0.553]	[0.553]	0.585 064 (32)	0.585 069 (37)		
Φ_I (Hz)	[0.000 226]	[0.000 226]	[0.000 000 240]	[0.000 000 240]		
Φ_{IK} (Hz)	[0.000 634]	[0.000 634]	[0.001 69]	[0.001 69]		
Φ_{KI} (Hz)	[-0.00281]	[-0.00281]	[-0.00391]	[-0.00391]		
Φ_K (Hz)	[0.002 63]	[0.002 63]	[0.003 35]	[0.003 35]		
$\phi_I (Hz)$	[0.000 100]	[0.000 100]	[0.000 000 120]	[0.000 000 120]		
ϕ_{IK} (Hz)	[0.000481]	[0.000 481]	[0.000 687]	[0.000 687]		
ϕ_K (Hz)	[0.000 663]	[0.000 663]	[0.001 08]	[0.001 08]		
$\Delta E_{23,24}$ (MHz)	591 678.7 (12)		596 970.65 (15)			
$\Delta E_{23,24} \text{ (cm}^{-1})$	19.736 276 (40)		19.912 797 4 (37)			
G_c^J (MHz)	0.006 13 (76)			060 (14)		
F_{ab} (MHz)	3.504 5 (10)			2.844 972 (78)		
$\Delta_i (u \mathring{A}^2)^{d,e}$	-0.2549 (11)	-0.247 28 (97)	-0.266 258 (4)	-0.238 738 (5)		
$\kappa^{\rm e}$	0.908	0.247 28 (57)	0.634	0.638		
$N_{ m lines}^{ m f}$	241	232	895	792		
	0.046	0.043	0.038	0.035		
$\sigma_{\rm fit}$ (MHz)	0.040	0.043	0.038	0.033		

^aColor-coding designates the type of vibrational motion (see Fig. 6) and not the vibrational state label. Vibrational state colors match Fig. 13, showing the corresponding vibrational motions of each isotopologue in the same color.

values are, unsurprisingly, in the constants with the smallest (<1 MHz) absolute value or from the isotopologues with highly correlated A- and B-rotational constants, e.g., [3-2H]-pyridazine. Due to the excellent agreement of the average values of the vibration-rotation interaction constants in these cases, we attribute this to the A_{ν} and B_{ν} values being highly correlated and not to poor theoretical treatment. It is likely that these discrepancies would be addressed by adding more transitions—especially with higher values of J and K_a —to the dataset, but these data are unfortunately not available. We are confident, however, in the $\Delta E_{23,24}$ value determined for each isotopologue, as a sufficient number of resonant transitions and nominal interstate transitions are included in the datasets. The reliability of the $\Delta E_{23,24}$ values is further supported by the observed consistency of these values during the least-squares fitting process. The vibration-rotation interaction constants for the three isotopologues that were not treated as a Coriolis-coupled dyad show excellent agreement between computed and experimental values (Table V). Combined with our observation *via* Loomis-Wood plots that the transition frequencies of these vibrational states are not significantly impacted by coupling perturbations in the frequency range studied, the agreement between the computed and experimental vibration-rotation interaction constants supports the choice to treat these states as distorted rotors.

Altogether, the analysis in this work illustrates three coupling situations for the two lowest-energy fundamental states of pyridazine isotopologues: (1) an energy separation too large to observe coupling between the states in our frequency region, (2) asymmetric isotopologues with a predominant F_{ab} term and potential for higher-order anharmonic coupling terms, and (3) symmetric isotopologues with only an F_{ab} term and the potential for higher-order coupling terms (or, in the case of the normal isotopologue, a predominant F_{ab} term with a smaller G_c). In the $G_{2\nu}$ isotopologues, the two vibrations have different symmetry (A2 and B1) and, therefore, can only

^bValues in brackets are held constant at their corresponding ground-state value.

^cHarmonic frequencies calculated using CCSD(T)/cc-pCVTZ.

^dInertial defect, $\Delta_i = I_c - I_a - I_b$.

^eCalculated using PLANM from the B_v constants.

^fNumber of fitted transition frequencies.

TABLE V. Vibration–rotation interaction constants and energy differences of the lowest-energy fundamental states of [²H]-pyridazine isotopologues. ^{a,b}

	$[3-^{2}H], C_{s}$		[4- ² H],	$[4-^{2}H], C_{s}$		$[3,4-^{2}H], C_{s}$	
	Experimental	CCSD(T) ^{c,4}	Experimental	CCSD(T) ^{c,4}	Experimental	CCSD(T) ^{c,4}	
$\begin{array}{c} A_0 - A_x \text{ (MHz)} \\ B_0 - B_x \text{ (MHz)} \\ C_0 - C_x \text{ (MHz)} \\ A_0 - A_y \text{ (MHz)} \\ B_0 - B_y \text{ (MHz)} \\ C_0 - C_y \text{ (MHz)} \end{array}$	1.708 (53) 5.262 (50) -3.198 29 (45) 3.315 (48) 3.078 (46) -3.234 28 (45)	2.636 4.406 -3.134 3.622 2.681 -3.210	3.831 23 (17) 4.015 26 (13) -3.166 812 (86) 7.065 06 (21) -0.814 58 (15) -3.299 042 (87)	3.787 4.059 -3.134 7.190 -0.925 -3.245	2.265 1 (14) 5.300 8 (17) -2.986 66 (36) 6.827 0 (17) -0.482 0 (21) -3.057 97 (36)	2.315 5.324 -2.938 6.846 -0.586 -3.027	
$\frac{(A_0 - A_x) + (A_0 - A_y)}{2}$ (MHz)	2.511 (72)	3.129	5.448 14 (27)	5.489	4.546 1 (22)	4.580	
$\frac{(B_0 - B_x) + (B_0 - B_y)}{2}$ (MHz)	4.170 (68)	3.544	1.600 34 (20)	1.567	2.409 4 (27)	2.369	
$\frac{(C_0 - C_x) + (C_0 - C_y)}{2}$ (MHz)	-3.216 29 (64)	-3.172	-3.232 93 (12)	-3.189	-3.022 31 (51)	-2.982	
$\Delta E_{\rm dyad} \ ({\rm cm}^{-1})^{\rm d}$ $G_c^J \ ({\rm MHz})$ $F_{ab} \ ({\rm MHz})$	19.736 276 (40) 0.006 13 (76) 3.504 5 (10)	16.1	-19.912 797 4 (37) 0.003 060 (14) 2.844 972 (78)	-22.5		25.1	
$N_{ m lines}^{ m \ e}$	241/232		895/792		276/262		
	[3,5- ² H]	$[3,5-^{2}H], C_{s}$		$[3,6-^{2}H], C_{2\nu}$		$[4,5-^{2}H], C_{2\nu}$	
	Experimental	CCSD(T) ^{c,4}	Experimental	CCSD(T) ^{c,4}	Experimental	CCSD(T) ^{c,4}	
$A_0 - A_x$ (MHz) $B_0 - B_x$ (MHz) $C_0 - C_x$ (MHz) $A_0 - A_y$ (MHz) $B_0 - B_y$ (MHz) $C_0 - C_y$ (MHz)	2.125 1 (40) 4.600 4 (44) -2.987 96 (37) 6.999 0 (18) 0.135 3 (31) -3.062 30 (39)	1.924 4.970 -2.931 7.256 -0.304 -3.039	3.300 3 (12) 4.028 7 (17) -2.975 43 (43) 4.745 5 (12) 1.423 8 (17) -3.067 87 (43)	3.163 4.191 -2.910 4.785 1.341 -3.057	3.748 02 (24) 4.295 81 (20) -2.974 35 (16) 7.539 44 (26) -1.067 59 (20) -3.104 53 (16)	3.741 4.240 -2.954 7.621 -1.055 -3.042	
$\frac{(A_0 - A_x) + (A_0 - A_y)}{2}$ (MHz)	4.562 1 (44)	4.590	4.022 9 (17)	3.974	5.643 73 (35)	5.681	
$\frac{(B_0 - B_x) + (B_0 - B_y)}{2}$ (MHz)	2.367 8 (54)	2.333	2.726 3 (25)	2.766	1.614 11 (29)	1.5922	
$\frac{(C_0 - C_x) + (C_0 - C_y)}{2}$ (MHz)	-3.025 13 (53)	-2.985	-3.0217 (61)	-2.984	-3.039 44 (22)	-2.998	
$\Delta E_{\text{dyad}} \text{ (cm}^{-1})^{\text{d}}$ $G_c^J \text{ (MHz)}$	9.274 460 (29) 0.002 36 (28)	7.4	(. ,	31.0	-17.088 984 6 (77)	-21.1	
F_{ab} (MHz) $N_{\rm lines}^{\rm e}$	1.676 10 (76) 245/226		208/179		2.070 99 (39) ^f 643/584		
	[3,4,5- ² H	[3,4,5- ² H], C _s		[3,4,6- ² H], C _s		$[3,4,5,6^{-2}H], C_{2\nu}$	
	Experimental	CCSD(T) ^{c,4}	Experimental	CCSD(T) ^{c,4}	Experimental	CCSD(T) ^{c,4}	
A_0-A_x (MHz) B_0-B_x (MHz) C_0-C_x (MHz) A_0-A_y (MHz) B_0-B_y (MHz) C_0-C_y (MHz)	4.433 27 (80) 3.004 68 (70) -2.845 32 (26) 4.511 75 (65) 2.033 39 (56) -2.851 59 (26)	3.991 3.536 -2.811 5.059 1.400 -2.810	2.156 16 (31) 4.897 18 (30) -2.804 16 (20) 6.466 72 (40) 0.291 99 (40) -2.886 06 (20)	2.045 5.056 -2.745 6.537 0.130 -2.872	1.931 7 (21) 4.614 4 (24) -2.678 01 (21) 4.559 1 (21) 2.588 2 (24) -2.683 04 (22)	1.910 4.673 -2.622 4.505 2.576 -2.674	
$\frac{(A_0 - A_x) + (A_0 - A_y)}{2}$ (MHz)	4.4725 (10)	4.525	4.311 44 (51)	4.292	3.245 4 (30)	3.208	
$\frac{(B_0 - B_x) + (B_0 - B_y)}{2}$ (MHz)	2.519 04 (90)	2.468	2.594 58 (50)	2.593	3.601 3 (34)	3.625	
$\frac{(C_0 - C_x) + (C_0 - C_y)}{2}$ (MHz)	-2.848 45 (37)	-2.810	-2.845 11 (28)	-2.808	-2.683 04 (31)	-2.648	
$\Delta E_{\rm dyad} ({\rm cm}^{-1})^{\rm d}$ $G_c^J ({\rm MHz})$	-9.267 386 5 (97)	-10.9		23.9	12.453 335 9 (37)	9.1	
F_{ab} (MHz) $N_{ m lines}^{ m e}$	0.841 (36) ^g 570/529		550/494		-2.355 965 (97) ^h 592/535		

 $[\]overline{{}^{a}\text{Vibrational states }\nu_{16}}$ (x) and ν_{13} (y) for $C_{2\nu}$ or ν_{24} (x) and ν_{23} (y) for C_{s} isotopologues.

^bColor-coding designates the type of vibrational motion (see Fig. 6) and not the vibrational state label. Vibrational state colors match Fig. 13, showing the corresponding vibrational motions of each isotopologue in the same color.

 $^{^{\}rm c}{\rm Evaluated}$ with the cc-pCVTZ basis set.

 $^{^{}d}\Delta E_{dyad}$ = energy of state corresponding to vibrational motion of v_{13} (Fig. 6(b); depicted in green in Figs. 6 and 13) - energy of state corresponding to vibrational motion of v_{16} (Fig. 6(a); depicted in purple in Figs. 6 and 13). In units of cm⁻¹. The vibrational state labels of v₁₆ and v₁₃ apply only for the case of C_{2v} isotopologues of pyridazine. Vibrational state labels change as a function of isotopic substitution for reasons of both symmetry and isotopic perturbation of vibrational modes.

^eNumber of fitted transition frequencies for [state x]/[state y].

fleast-squares fit includes $F_{ab}{}^{I} = -0.000\,006\,84\,(16)\,\text{MHz}$ and $F_{ab}{}^{K} = 0.000\,005\,54\,(36)\,\text{MHz}$. g Least-squares fit includes $F_{ab}{}^{K} = -0.000\,024\,2\,(15)\,\text{MHz}$ and $W^{K} = 2.796\,(47)\,\text{MHz}$. h Least-squares fit includes $F_{ab}{}^{I} = 0.000\,003\,763\,(41)\,\text{MHz}$.

be coupled by Coriolis interactions. For the C_s isotopologues, both vibrations have A" symmetry; therefore, anharmonic coupling is possible. Because no computational estimates are available for the dyad coupling constants of any of the isotopologues, analysis of each dyad was begun using coupling terms of an analogous dyad when available, and transitions were added until evidence of coupling was observed.

For dyads of the first type mentioned earlier, all observable transitions were least-squares fit to these two distorted-rotor states without the need for a coupling term. If a coupling term was allowed to fit, it fit to near-zero with an uncertainty larger than its value. In the latter two cases, the coupling fortuitously resulted in resonances, which appeared as gaps in Loomis-Wood plots and as gaps with no measured transitions in resonance plots. Attempts to fit the energy separation and predominant coupling terms, however, did not result in the refinement of these terms in a manner than predicted either the frequencies of these missing transitions or even resonances at the proper locations. At this point, the energy separation was manually adjusted, a corresponding prediction file was generated, and a resonance plot with an expected resonance was examined. We continued to adjust the energy separation until a resonance appeared in the expected *J* range of the resonance plot. With this better estimate of the energy separation, the least-squares fitting routine was able to refine the energy separation and predominant coupling term to better predict the missing transition frequencies.

Further fitting proceeded more typically by adding transitions that enabled refinement of the spectroscopic terms until all observable transitions were incorporated. When additional coupling terms beyond the predominant term were necessary, the theoretically possible coupling terms for any given dyad were tested in the fit. The constant that could be determined and best fit the data was maintained in the final least-squares fit. In some cases, multiple constants (often G_c^J and F_{ab}^K) were able to produce similarly low-error leastsquares fits incorporating all of the same data. In these cases, G_c^J was used to produce least-squares fits that are relatively comparable across the series of isotopologues. Although use of the anharmonic coupling (W^I) and W^K) terms was attempted in the fitting of each Cs dyad, only one dyad was able to employ such a constant: the v_{24} - v_{23} dyad of [3,4,5- 2 H]-pyridazine required F_{ab} , $F_{ab}^{\ \ K}$, and W^K for a low-error least-squares fit. As is shown in Table V, there is some similarity between the coupling terms of the dyads for which coupling was observed, and in each case, the coupling terms employed were sufficient to fit the observed resonances. In each of the dyad fits, the $|F_{ab}|$ value is between 1.5 and 3.7 MHz, with the exception of [3,4,5-2H]-pyridazine—the only dyad to use an anharmonic coupling term. The smaller $|G_c|$ values are between 0.002 and 0.007 MHz. There is not, however, sufficient consistency in the analysis to provide any definitive conclusion, except perhaps the magnitude of the coupling term to expect when fitting. In this regard, this analysis will be useful for future least-squares fitting of similar dyads. Once the dyad of one isotopologue has been established, the corresponding dyads of other isotopologues are likely to have similar coupling term values. The exact terms that will be necessary, however, are still not readily predictable a priori by either computational software or historically built-up experimental data. Taking into account that similarly high-quality least-squares fits for several of the pyridazine dyads discussed in this work could be achieved using a different set of coupling parameters, the parameters and values reported here should be considered to be largely empirical.

By analyzing the analogous vibrational modes for all of the pyridazine- d_x isotopologues, we gain direct insight into the impact of isotopic substitution on the energy difference between the two ring-deformation vibrational modes. The two lowest-energy fundamental states of three species, $[3,4^{-2}H]$ -, $[3,6^{-2}H]$ -, and $[3,4,6^{-2}H]$ pyridazine, were able to be least-squares fit adequately to single-state models and did not show any obvious signs of Coriolis coupling between states across the observed frequency range. Undoubtedly, if the frequency coverage were extended, these states would begin to show noticeable perturbations of transition frequencies. These three isotopologues have the largest computed harmonic ΔE values, all greater than 24 cm⁻¹. This value is approximately the minimum energy separation necessary for pyridazine isotopologues to have unperturbed transition frequencies between 235 and 360 GHz. For all other isotopologues, these two vibrationally excited states required the use of a two-state Hamiltonian model. The resulting ΔE values and their corresponding computed values are provided in Table V and plotted in Fig. 14. As mentioned earlier, the Cartesian coordinates of the normal coordinate analysis were used to confirm that the analogous vibrational motions were being treated consistently.

As discussed previously, the computed values of v_{16} and v_{13} of the normal isotopologue incorrectly predict the lowest-energy fundamental as v_{13} rather than v_{16} . The fundamental frequency of ν_{13} is overpredicted by 3 cm⁻¹ and ν_{16} is overpredicted by 8 cm⁻¹ (Table II). This is the only isotopologue for which the discrepancy can be assigned to one or both vibrationally excited states - a consequence of having the high-resolution infrared analysis. It is also the only isotopologue for which a complete anharmonic vibrational calculation providing the fundamental frequencies has been completed. The computed harmonic and fundamental ΔE values for these states are very similar (4.52 and 4.54 cm⁻¹, respectively). The harmonic and fundamental computed ΔE values of pyridazine differ by 0.02 cm^{-1} , far less than the |obs.-calc.| value of 4.59 cm⁻¹. Therefore, we assume that any discrepancies observed between the harmonic and experimental ΔE values are not due to the lack of anharmonic treatment for the other isotopologues. The root mean square (rms) error in the computed ΔE values is 3.2 cm⁻¹ and, as shown in Table V and Fig. 14, the individual values are sometimes overpredicted and sometimes underpredicted. The absolute values of the difference between the computed harmonic and experimental ΔE values are all less than 5 cm⁻¹, with the largest | obs.-calc.| value being that for the normal isotopologue. The accuracy of the computed values depends on the accuracy of the equilibrium geometry and the force constants used to determine the vibrational frequency. Given that the equilibrium geometry is nearly identical for isotopologues regardless of H/D substitution, 23,24 all isotopologues would be impacted in an identical manner if there were substantial systematic errors in the equilibrium geometry. This implies that most of the error in the computed harmonic ΔE values must come from the determination of the harmonic force constants.

As is evident in Fig. 14, mono-substitution of 1H by 2H in pyridazine has the largest impact on the ΔE value, regardless of position. Deuterium substitution at the 3-position increases the ΔE value, while substitution at the 4-position reduces the ΔE value. Subsequent deuterium substitution, regardless of location, reduces

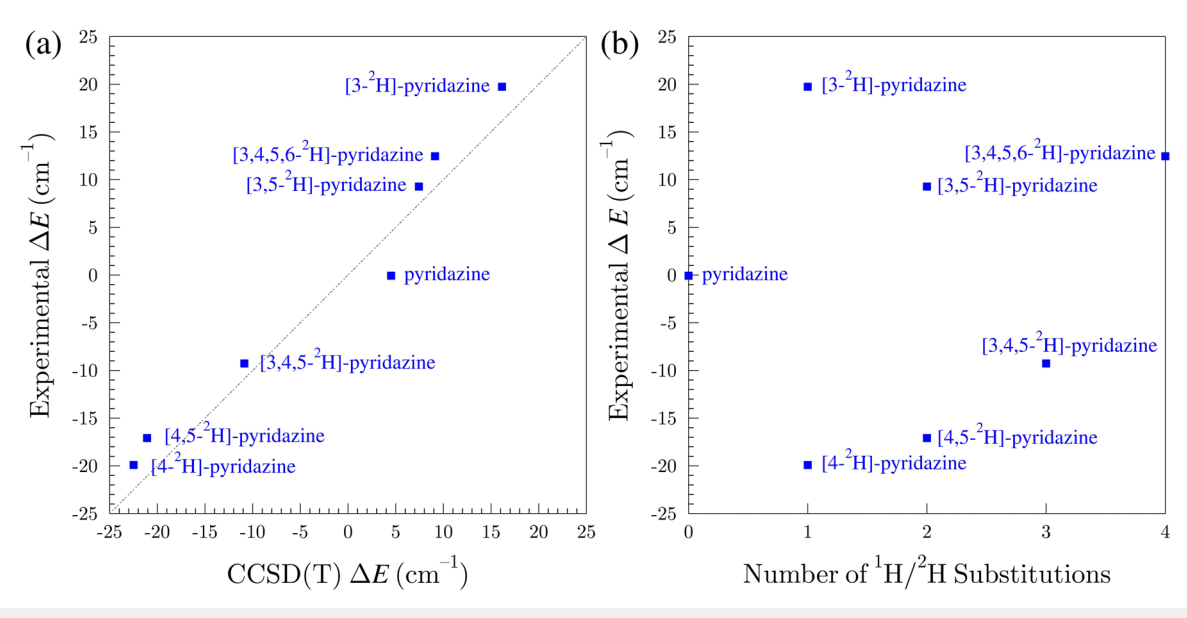


FIG. 14. (a)Experimental energy difference of the two lowest-energy fundamental states of pyridazine determined by least-squares fitting of the Coriolis-coupled dyad (ΔE_{dyad} , Table V; in cm⁻¹) vs. computed energy difference, and (b) experimental ΔE vs. the number of $^{1}\text{H}/^{2}\text{H}$ substitutions. The gray dashed line represents an ideal correlation between computed and experimental energy differences. The three isotopologues that did not have perturbed transition frequencies ([3,4- ^{2}H]-, [3,6- ^{2}H]-, and [3,4,6- ^{2}H]-pyridazine) are not included in these plots.

the absolute value of ΔE . Isotopologues with deuterium substitutions at the 3- or the equivalent 6-position tend toward $E_{16} < E_{13}$, while isotopologues with substitutions at the 4- or the equivalent 5-position have the opposite effect ($E_{13} < E_{16}$). The per-deuterio isotopologue ([3,4,5,6-2H]-pyridazine), which has equal substitutions at the 3/6 and 4/5 positions, has a positive ΔE value. Inspection of the substitution patterns on the harmonic frequencies of the v_{13} and v₁₆-equivalent modes independently reveals a few trends that help explain the observed ΔE values. Deuterium substitution at the 3/6 position has a predicted monotonic decrease in the vibrational frequency of the v₁₆-equivalent modes, while deuterium substitution at the 4/5 position has a predicted monotonic decrease in the vibrational frequency of the v_{13} -equivalent modes. There is no consistent impact of 3/6 position deuterium substitution on the v_{13} -equivalent modes or 4/5 position deuterium substitution on the v_{16} -equivalent modes. Not surprisingly, the v_{13} -equivalent modes have a larger, out-of-plane displacement of the 4/5 hydrogen atoms and smaller movements of the 3/6 hydrogen atoms. In contrast, the v_{16} -equivalent modes have a larger, out-of-plane displacement of the 3/6 hydrogen atoms and smaller movements of the 4/5 hydrogen atoms.

CONCLUSION

The rotational transition frequencies of pyridazine presented in this work from 8 to 18 and 130 to 750 GHz, combined with the previous measurements, provide the foundation for future searches for pyridazine in extraterrestrial environments. The newly expanded frequency range provides experimental frequencies that cover a large

portion of the spectrum available to modern radiotelescopes. The detection of pyridazine, or any other aromatic heterocycle, would be a dramatic advance in understanding the chemistry of the interstellar medium. Transition frequencies not directly measured but within the bounds of the frequency ranges observed in this work should be predicted within experimental measurement uncertainty by the spectroscopic constants presented in this work. The transition frequencies well above 750 GHz will likely not be predicted as accurately, as transitions with those *J/K* values are not included in this work.

Investigation of the pyridazine coupled dyads (v_{16} - v_{13} and v_{24} v₉) provides definitive band origins for each of these vibrationally excited states, which highlights the power of combining millimeterwave with high-resolution infrared transitions into a single dataset. Transitions from both techniques provide information regarding the rotational and centrifugal distortion constants, because they cover similar J/K_a ranges, albeit at different resolutions. Analysis of the rotational data provides the energy difference between the states via the Corolis-coupling interactions, but cannot locate the band origins of any vibrational state. The high-resolution infrared data provide the band origin for the two intense fundamental states $(v_{16} \text{ and } v_9)$, but transitions associated with v_{13} and v_{24} cannot be observed. When combined, the band origins of all four fundamental states can be obtained with high accuracy and precision. The high-quality determination of the energy differences and spectroscopic constants for these states provides important benchmarks for computational chemists with two distinct types of Coriolis-coupled dyads. The lower-energy dyad of v_{16} and v_{13} has a remarkably small energy separation [0.070 789 7 (24) cm⁻¹] and c-axis coupling

without a Coriolis ζ^c constant, while the higher-energy dyad of v_{24} and v_9 has a large energy separation and a distinctly non-zero ζ^c constant. The difference between the computed and observed energy separations for each of these dyads is approximately 4 cm^{-1} . While this value represents a relatively small error, it has a substantial impact on the *a priori* prediction of the rotational spectra due to the Coriolis coupling.

By analyzing the same vibrational modes across all ten ¹H/²Hisotopologues of pyridazine, we created an interesting new type of dataset for computational benchmarking. These isotopologues provide a large number of vibration-rotation interaction, centrifugal distortion, and Coriolis-coupling constants that can be used as benchmarks. Many of these constants are adequately reproduced by the CCSD(T) calculations employed in this work. The experimental impact of ¹H/²H substitution on the vibrational energy separation is determined for seven isotopologues, and a lower bound for the two lowest-energy vibrationally excited states of the other three isotopologues is established. These values are reasonably predicted by the coupled-cluster method employed, but with apparent small inadequacies in the computation of both quadratic and higher-order force constants. Accurate prediction of the vibrational energies of the two lowest-energy fundamental states and their centrifugal distortion constants remains a substantial challenge to readily available computational packages or methodologies.

SUPPLEMENTARY MATERIAL

Computational chemistry output files and least-squares fitting output files from SPFIT are provided in the supplementary material.

ACKNOWLEDGMENTS

We gratefully acknowledge funding from the U.S. National Science Foundation for support of this project (Grant Nos. CHE-2245738 and CHE-1954270). Part of the research described in this paper was performed at the Canadian Light Source, a national research facility of the University of Saskatchewan, which is supported by the Canada Foundation for Innovation (CFI), the Natural Sciences and Engineering Research Council (NSERC), the National Research Council (NRC), the Canadian Institutes of Health Research (CIHR), the Government of Saskatchewan, and the University of Saskatchewan. We acknowledge Michael McCarthy for the loan of an amplification-multiplication chain. We acknowledge John Stanton for his thoughtful conversations.

AUTHOR DECLARATIONS

Conflict of Interest

The authors have no conflicts to disclose.

Author Contributions

Brian J. Esselman: Conceptualization (equal); Formal analysis (equal); Investigation (equal); Writing – original draft (equal); Writing – review & editing (equal). **Maria A. Zdanovskaia**: Formal analysis (equal); Investigation (equal); Writing – original draft (equal);

Writing – review & editing (equal). Brent K. Amberger: Formal analysis (equal); Investigation (equal); Writing – review & editing (equal). Joshua D. Shutter: Formal analysis (equal); Investigation (equal); Writing – review & editing (equal). Andrew N. Owen: Formal analysis (equal); Writing – review & editing (equal). Brant E. Billinghurst: Formal analysis (equal); Investigation (equal); Resources (equal); Writing – review & editing (equal). Jianbao Zhao: Formal analysis (equal); Investigation (equal); Resources (equal); Writing – review & editing (equal). Zbigniew Kisiel: Formal analysis (equal); Investigation (equal); Writing – review & editing (equal). R. Claude Woods: Conceptualization (equal); Formal analysis (equal); Investigation (equal); Supervision (equal); Writing – review & editing (equal). Robert J. McMahon: Funding acquisition (equal); Investigation (equal); Supervision (equal); Writing – review & editing (equal).

DATA AVAILABILITY

The data that support the findings of this study are available within the article and its supplementary material.

REFERENCES

- ¹ W. Werner, H. Dreizler, and H. D. Rudolph, "Zum mikrowellenspektrum des pyridazins," Z. Naturforsch. A **22**, 531–543 (1967).
- ²J. C. López, A. de Luis, S. Blanco, A. Lesarri, and J. L. Alonso, "Investigation of the quadrupole coupling hyperfine structure due to two nuclei by molecular beam Fourier transform microwave spectroscopy: Spectra of dichlorofluoromethane and pyridazine," J. Mol. Struct. 612, 287–303 (2002).
- ³B. J. Esselman, B. K. Amberger, J. D. Shutter, M. A. Daane, J. F. Stanton, R. C. Woods, and R. J. McMahon, "Rotational spectroscopy of pyridazine and its isotopologs from 235–360 GHz: Equilibrium structure and vibrational satellites," J. Chem. Phys. 139, 224304 (2013).
- ⁴A. N. Owen, M. A. Zdanovskaia, B. J. Esselman, J. F. Stanton, R. C. Woods, and R. J. McMahon, "Semi-experimental equilibrium (r_e^{SE}) and theoretical structures of pyridazine (o-C₄H₄N₂)," J. Phys. Chem. A **125**, 7976–7987 (2021).
- ⁵Y.-J. Kuan, C.-H. Yan, S. B. Charnley, Z. Kisiel, P. Ehrenfreund, and H.-C. Huang, "A search for interstellar pyrimidine," Mon. Not. R. Astron. Soc. **345**, 650–656 (2003).
- ⁶T. J. Barnum, M. A. Siebert, K. L. K. Lee, R. A. Loomis, P. B. Changala, S. B. Charnley, M. L. Sita, C. Xue, A. J. Remijan, A. M. Burkhardt, B. A. McGuire, and I. R. Cooke, "A search for heterocycles in GOTHAM observations of TMC-1," J. Phys. Chem. A 126, 2716–2728 (2022).
- ⁷B. A. McGuire, A. M. Burkhardt, S. Kalenskii, C. N. Shingledecker, A. J. Remijan, E. Herbst, and M. C. McCarthy, "Detection of the aromatic molecule benzonitrile (c- C_6 H $_5$ CN) in the interstellar medium," Science **359**, 202–205 (2018).
- ⁸S. B. Charnley, Y.-J. Kuan, H.-C. Huang, O. Botta, H. M. Butner, N. Cox, D. Despois, P. Ehrenfreund, Z. Kisiel, Y.-Y. Lee, A. J. Markwick, Z. Peeters, and S. D. Rodgers, "Astronomical searches for nitrogen heterocycles," Adv. Space Res. 36, 137–145 (2005).
- ⁹M. N. Simon and M. Simon, "Search for interstellar acrylonitrile, pyrimidine, and pyridine," Astrophys. J. **184**, 757–761 (1973).
- ¹⁰M. Lattelais, Y. Ellinger, A. Matrane, and J.-C. Guillemin, "Looking for heteroaromatic rings and related isomers as interstellar candidates," Phys. Chem. Chem. Phys. 12, 4165–4171 (2010).
- ¹¹M. L. Kutner, D. E. Machnik, K. D. Tucker, and R. L. Dickman, "Search for interstellar pyrrole and furan," Astrophys. J. 242, 541–544 (1980).
- ¹²P. Pulay, W. Meyer, and J. E. Boggs, "Cubic force constants and equilibrium geometry of methane from Hartree–Fock and correlated wavefunctions," J. Chem. Phys. 68, 5077–5085 (1978).

- ¹³ J. Vázquez and J. F. Stanton, "Semiexperimental equilibrium structures computational aspects," in *Equilibrium Molecular Structures: From Spectroscopy to Quantum Chemistry*, edited by J. Demaison, J. E. Boggs, and A. G. Császár (Taylor & Francis Group: CRC Press, 2010), pp. 53–87.
- ¹⁴C. Puzzarini, "Accurate molecular structures of small- and medium-sized molecules," Int. J. Quantum Chem. 116, 1513–1519 (2016).
- ¹⁵C. Puzzarini and V. Barone, "Diving for accurate structures in the ocean of molecular systems with the help of spectroscopy and quantum chemistry," Acc. Chem. Res. **51**, 548–556 (2018).
- ¹⁶C. Puzzarini and J. F. Stanton, "Connections between the accuracy of rotational constants and equilibrium molecular structures," Phys. Chem. Chem. Phys. 25, 1421–1429 (2023).
- ¹⁷M. A. Zdanovskaia, B. J. Esselman, S. M. Kougias, B. K. Amberger, J. F. Stanton, R. C. Woods, and R. J. McMahon, "Precise equilibrium structures of 1*H* and 2*H*-1,2,3-triazoles (C₂H₃N₃) by millimeter-wave spectroscopy," J. Chem. Phys. 157, 084305 (2022).
- 18 A. N. Owen, N. P. Sahoo, B. J. Esselman, J. F. Stanton, R. C. Woods, and R. J. McMahon, "Semi-experimental equilibrium ($r_{\rm e}^{\rm SE}$) and theoretical structures of hydrazoic acid (HN₃)," J. Chem. Phys. 157, 034303 (2022).
- 19 H. A. Bunn, B. J. Esselman, P. R. Franke, S. M. Kougias, R. J. McMahon, J. F. Stanton, S. L. Widicus Weaver, and R. C. Woods, "Millimeter/submillimeter-wave spectroscopy and the semi-experimental equilibrium (r_e^{SE}) structure of 1H-1,2,4-triazole (c- $C_2H_3N_3$)," J. Phys. Chem. A 126, 8196–8210 (2022).
- ²⁰ V. L. Orr, Y. Ichikawa, A. R. Patel, S. M. Kougias, K. Kobayashi, J. F. Stanton, B. J. Esselman, R. C. Woods, and R. J. McMahon, "Precise equilibrium structure determination of thiophene (*c*-C₄H₄S) by rotational spectroscopy—Structure of a five-membered heterocycle containing a third-row atom," J. Chem. Phys. 154, 244310 (2021).
- ²¹ B. J. Esselman, M. A. Zdanovskaia, A. N. Owen, J. F. Stanton, R. C. Woods, and R. J. McMahon, "Precise equilibrium structure of thiazole (c-C₃H₃NS) from twenty-four isotopologues," J. Chem. Phys. 155, 054302 (2021).
- ²²Z. N. Heim, B. K. Amberger, B. J. Esselman, J. F. Stanton, R. C. Woods, and R. J. McMahon, "Molecular structure determination: Equilibrium structure of pyrimidine $(m\text{-}\mathrm{C}_4\mathrm{H}_4\mathrm{N}_2)$ from rotational spectroscopy (r_e^{SE}) and high-level *ab initio* calculation (r_e) agree within the uncertainty of experimental measurement," J. Chem. Phys. **152**, 104303 (2020).
- ²³B. J. Esselman, M. A. Zdanovskaia, A. N. Owen, J. F. Stanton, R. C. Woods, and R. J. McMahon, "Precise equilibrium structure of benzene," J. Am. Chem. Soc. 145, 21785–21797 (2023).
- ²⁴H. H. Smith, B. J. Esselman, S. A. Wood, J. F. Stanton, R. C. Woods, and R. J. McMahon, "Improved semi-experimental equilibrium structure and high-level theoretical structures of ketene," J. Chem. Phys. **158**, 244304 (2023).
- ²⁵ H. Takahashi, K. Mamola, and E. K. Plyler, "Effects of hydrogen bond formation on vibrations of pyridine, pyrazine, pyrimidine, and pyridazine," J. Mol. Spectrosc. **21**, 217–230 (1966).
- ²⁶H. D. Stidham and J. V. Tucci, "Vibrational spectra of pyridazine, pyridazine- d_4 , pyridazine-3,6- d_2 and pyridazine-4,5- d_2 ," Spectrochim. Acta, Part A 23, 2233–2242 (1967).
- ²⁷Y. Ozono, Y. Nibu, H. Shimada, and R. Shimada, "Polarized Raman and infrared spectra of [¹H₄]- and [²H₄]-pyridazines," Bull. Chem. Soc. Jpn. **59**, 2997–3001 (1986).
- ²⁸F. Billes, H. Mikosch, and S. Holly, "A comparative study on the vibrational spectroscopy of pyridazine, pyrimidine and pyrazine," J. Mol. Struct.: THEOCHEM 423, 225–234 (1998).
- ²⁹ J. Vázquez, J. J. L. Gozález, F. Márquez, and J. E. Boggs, "Vibrational spectrum of pyridazine," J. Raman Spectrosc. **29**, 547–559 (1998).
- ³⁰P. M. Higgins, B. J. Esselman, M. A. Zdanovskaia, R. C. Woods, and R. J. McMahon, "Millimeter-wave spectroscopy of the chlorine isotopologues of chloropyrazine and twenty-two of their vibrationally excited states," J. Mol. Spectrosc. **364**, 111179 (2019).
- ³¹B. J. Esselman, M. A. Zdanovskaia, R. C. Woods, and R. J. McMahon, "Millimeter-wave spectroscopy of the chlorine isotopologues of 2-chloropyridine and twenty-three of their vibrationally excited states," J. Mol. Spectrosc. 365, 111206 (2019).
- ³²I. Uriarte, Z. Kisiel, E. Białkowska-Jaworska, L. Pszczółkowski, P. Ecija, F. J. Basterretxea, and E. J. Cocinero, "Comprehensive rotational spectroscopy of the

- newly identified atmospheric ozone depleter CF_3CH_2Cl ," J. Mol. Spectrosc. 337, 37–45 (2017).
- ³³O. Dorosh, E. Białkowska-Jaworska, Z. Kisiel, and L. Pszczółkowski, "New measurements and global analysis of rotational spectra of Cl-, Br-, and I-benzene: Spectroscopic constants and electric dipole moments," J. Mol. Spectrosc. 246, 228–232 (2007).
- ³⁴E. Białkowska-Jaworska, L. Pszczółkowski, and Z. Kisiel, "Comprehensive analysis of the rotational spectrum of 2,2-dichloropropane," J. Mol. Spectrosc. 308–309, 20–27 (2015).
- 35 R. A. H. Butler, D. T. Petkie, P. Helminger, F. C. De Lucia, E. Bialkowska-Jaworska, and Z. Kisiel, "The millimeter-wave spectrum of chlorine nitrate (ClONO₂): The v_6 vibrational state," J. Mol. Spectrosc. **244**, 113–116 (2007).
- ³⁶P. M. Dorman, B. J. Esselman, P. B. Changala, M. C. McCarthy, R. C. Woods, and R. J. McMahon, "Rotational spectra of twenty-one vibrational states of [³⁵Cl]-and [³⁷Cl]-chlorobenzene," J. Mol. Spectrosc. **394**, 111776 (2023).
- ³⁷M. A. Zdanovskaia, P. R. Franke, B. J. Esselman, B. E. Billinghurst, J. Zhao, J. F. Stanton, R. C. Woods, and R. J. McMahon, "Vibrationally excited states of 1*H* and 2*H*-1,2,3-triazole isotopologues analyzed by millimeter-wave and high-resolution infrared spectroscopy with approximate state-specific quartic distortion constants," J. Chem. Phys. 158, 044301 (2023).
- 38 Z. Kisiel, E. Białkowska-Jaworska, and L. Pszczółkowski, "The ∠ICI bending satellites in the millimeter-wave rotational spectra of CH₂I₂ and CD₂I₂," J. Mol. Spectrosc. **199**, 5–12 (2000).
- ³⁹B. K. Amberger, B. J. Esselman, J. F. Stanton, R. C. Woods, and R. J. McMahon, "Precise equilibrium structure determination of hydrazoic acid (HN₃) by millimeter-wave spectroscopy," J. Chem. Phys. **143**, 104310 (2015).
- ⁴⁰Z. Kisiel and E. Białkowska-Jaworska, "Sextic centrifugal distortion in fluorobenzene and phenylacetylene from cm-wave rotational spectroscopy," J. Mol. Spectrosc. 359, 16–21 (2019).
- ⁴¹ M. Krüger and H. Dreizler, "A microwave Fourier transform spectrometer with a single microwave Source," Z. Naturforsch. A **45**, 724–726 (1990).
- ⁴²M. Krüger, H. Harder, C. Gerke, and H. Dreizler, "Notizen: An automatic scan waveguide microwave Fourier transform spectrometer," Z. Naturforsch. A **48**, 737–738 (1993).
- 43 Z. Kisiel, "Further rotational spectroscopy of phenol: Sextic centrifugal distortion and vibrational satellites," J. Mol. Spectrosc. **386**, 111630 (2022).
- ⁴⁴Z. Kisiel, L. Pszczółkowski, B. J. Drouin, C. S. Brauer, S. Yu, J. C. Pearson, I. R. Medvedev, S. Fortman, and C. Neese, "Broadband rotational spectroscopy of acrylonitrile: Vibrational energies from perturbations," J. Mol. Spectrosc. 280, 134–144 (2012).
- ⁴⁵Z. Kisiel, L. Pszczółkowski, I. R. Medvedev, M. Winnewisser, F. C. De Lucia, and E. Herbst, "Rotational spectrum of *trans-trans* diethyl ether in the ground and three excited vibrational states," J. Mol. Spectrosc. 233, 231–243 (2005).
- 46 H. M. Pickett, "The fitting and prediction of vibration-rotation spectra with spin interactions," J. Mol. Spectrosc. **148**, 371–377 (1991).
- ⁴⁷Z. Kisiel, "Assignment and analysis of complex rotational spectra," in *Spectroscopy from Space*, edited by J. Demaison, K. Sarka, and E. A. Cohen (Kluwer Academic Publishers, Dordrecht, 2001), pp. 91–106.
- ⁴⁸See http://info.ifpan.edu.pl/~kisiel/prospe.htm for PROSPE—Programs for ROtational SPEctroscopy.
- ⁴⁹J. F. Stanton, J. Gauss, M. E. Harding, P. G. Szalay, with contribution from, R. J. Bartlett, A. A. Auer, U. Benedikt, C. Berger, D. E. Bernholdt, Y. J. Bomble, L. Cheng, O. Christiansen, M. Heckert, O. Heun, C. Huber, T.-C. Jagau, D. Jonsson, J. Jusélius, K. Klein, W. J. Lauderdale, D. A. Matthews, T. Metzroth, L. A. Mück, D. P. O'Neill, D. R. Price, E. Prochnow, C. Puzzarini, K. Ruud, F. Schiffmann, W. Schwalbach, S. Stopkowicz, A. Tajti, J. Vázquez, F. Wang, J. D. Watts, and the integral packages MOLECULE (J. Almlöf and P. R. Taylor), PROPS (P. R. Taylor), ABACUS (T. Helgaker, H. J. A. Jensen, P. Jørgensen, and J. Olsen), and ECP routines by A. V. Mitin and C. van Wüllen. For the current version, see http://www.cfour.de.
- ⁵⁰I. M. Mills, "Vibration-rotation structure in asymmetric and symmetric top molecules," in *Molecular Spectroscopy: Modern Research*, edited by K. N. Rao and C. W. Mathews (Academic Press, New York, 1972), Vol. 1, pp. 115–140.

- ⁵¹W. Schneider and W. Thiel, "Anharmonic force fields from analytic second derivatives: Method and application to methyl bromide," Chem. Phys. Lett. 157, 367–373 (1989).
- ⁵²J. F. Stanton, C. L. Lopreore, and J. Gauss, "The equilibrium structure and fundamental vibrational frequencies of dioxirane," J. Chem. Phys. **108**, 7190–7196 (1998).
- ⁵³J. K. G. Watson, "Aspects of quartic and sextic centrifugal effects on rotational energy levels," in *Vibrational Spectra and Structure*, edited by J. R. During (Elsevier, Amsterdam, 1977), Vol. 6, pp. 1–89.
- ⁵⁴J. K. G. Watson, "Determination of centrifugal distortion coefficients of asymmetric-top molecules," J. Chem. Phys. 46, 1935–1949 (1967).
- ⁵⁵ M. A. Zdanovskaia, B. J. Esselman, H. S. Lau, D. M. Bates, R. C. Woods, R. J. McMahon, and Z. Kisiel, "The 103–360 GHz rotational spectrum of benzonitrile, the first interstellar benzene derivative detected by radioastronomy," J. Mol. Spectrosc. 351, 39–48 (2018).
- 56 B. J. Esselman, M. A. Zdanovskaia, T. K. Adkins, B. E. Billinghurst, J. Zhao, R. C. Woods, and R. J. McMahon, "Millimeter-wave and infrared spectroscopy of thiazole (c-C₃H₃NS) in its ground state and lowest-energy vibrationally excited states (v_{18} , v_{17} , and v_{13})," J. Mol. Spectrosc. 379, 111493 (2021).
- ⁵⁷T. J. Barnum, K. L. K. Lee, and B. A. McGuire, "Chirped-pulse Fourier transform millimeter-wave spectroscopy of furan, isotopologues, and vibrational excited states," ACS Earth Space Chem. 5, 2986–2994 (2021).
- 58 D. W. Tokaryk, S. D. Culligan, B. E. Billinghurst, and J. A. van Wijngaarden, "Synchrotron-based far-infrared spectroscopy of furan: Rotational analysis of the v_{14} , v_{11} , v_{18} and v_{19} vibrational levels," J. Mol. Spectrosc. **270**, 56–60 (2011).
- ⁵⁹ M. A. Zdanovskaia, M.-A. Martin-Drumel, Z. Kisiel, O. Pirali, B. J. Esselman, R. C. Woods, and R. J. McMahon, "The eight lowest-energy vibrational states of

- benzonitrile: Analysis of Coriolis and Darling-Dennison couplings by millimeterwave and far-infrared spectroscopy," J. Mol. Spectrosc. 383, 111568 (2022).
- 60 H. H. Smith, S. M. Kougias, B. J. Esselman, R. C. Woods, and R. J. McMahon, "Synthesis, purification, and rotational spectroscopy of 1-cyanocyclobutene (C_5H_5N)," J. Phys. Chem. A **126**, 1980–1993 (2022).
- 61 B. J. Esselman, M. A. Zdanovskaia, H. H. Smith, R. C. Woods, and R. J. McMahon, "The 130–500 GHz rotational spectroscopy of cyanopyrazine ($C_4H_3N_2$ -CN)," J. Mol. Spectrosc. **389**, 111703 (2022).
- ⁶²M. A. Zdanovskaia, B. J. Esselman, S. M. Kougias, A. R. Patel, R. C. Woods, and R. J. McMahon, "The 130–360 GHz rotational spectrum of *syn-2-cyano-1,3-butadiene* (C₅H₅N)—A molecule of astrochemical relevance," Mol. Phys. **119**, e1964629 (2021).
- ⁶³B. J. Esselman, S. M. Kougias, M. A. Zdanovskaia, R. C. Woods, and R. J. McMahon, "Synthesis, purification, and rotational spectroscopy of (cyanomethylene)cyclopropane—An isomer of pyridine," J. Phys. Chem. A 125, 5601–5614 (2021).
- ⁶⁴P. M. Dorman, B. J. Esselman, R. C. Woods, and R. J. McMahon, "An analysis of the rotational ground state and lowest-energy vibrationally excited dyad of 3-cyanopyridine: Low symmetry reveals rich complexity of perturbations, couplings, and interstate transitions," J. Mol. Spectrosc. 373, 111373 (2020).
- 65 P. M. Dorman, B. J. Esselman, J. E. Park, R. C. Woods, and R. J. McMahon, "Millimeter-wave spectrum of 4-cyanopyridine in its ground state and lowest-energy vibrationally excited states, ν_{20} and ν_{30} ," J. Mol. Spectrosc. **369**, 111274 (2020).
- 66 M. A. Zdanovskaia, B. J. Esselman, R. C. Woods, and R. J. McMahon, "The 130–370 GHz rotational spectrum of phenyl isocyanide (C₆H₅NC)," J. Chem. Phys. 151, 024301 (2019).